REPUBLIC OF TURKEY

ACIBADEM MEHMET ALİ AYDINLAR UNIVERSITY
INSTITUTE OF NATURAL AND APPLIED SCIENCES

# PREPARATION OF DRUG LOADED NANOPARTICLES AND THEIR INCORPORATION INTO THERMOSENSITIVE HYDROGELS AS INJECTABLE DRUG DELIVERY SYSTEMS

ELİF GÜLİN ERTUĞRAL

MASTER THESIS

DEPARTMENT OF MEDICAL ENGINEERING

SUPERVISOR

Assist. Prof. Özgül GÖK

ISTANBUL – 2020

TEZ ONAY SAYFASI

# DECLARATION

I declare that this thesis has been composed by myself and it has not been submitted in any previous application for any other degree. Except collaborative contributions, the experimental work and the data analysis were entirely done by my own. References have been used for supporting literatures.

Elif Gülin Ertuğral

# TABLE OF CONTENT

**DECLARATION**..... iii
**TABLE OF CONTENT**..... iv
**ACKNOWLEDGMENT** ..... vii
**LIST OF ABBREVIATIONS** ..... viii
**LIST OF FIGURES** ..... ix
**LIST OF TABLES** ..... xiii
**SUMMARY** ..... 1
**ÖZET**..... 3
**1.BACKGROUND AND AIM OF THE STUDY** ..... 5
**2.INTRODUCTION**..... 7
**2.1.Drug Delivery Systems (DDSs)** ..... 7
**2.1.1.Nanoparticles (NPs)** ..... 9
**2.1.1.1.Polymeric Nanoparticles**..... 10
**2.1.2 Targeted Nanoparticles** ..... 11
**2.1.3. Functionalization**..... 13
**2.1.4. Drug Loading**..... 14
**2.1.5. Hydrogels** ..... 15
**2.1.6. Nanoparticle Embedded Hydrogel Scaffolds as DDS**..... 19
**3.MATERIALS AND METHODS** ..... 21
**3.1.Materials** ..... 21
**3.2.Preparation of Drug Delivery Systems**..... 22
**3.2.1.Preparation of Alginate Nanoparticles (AA-NPs)**..... 22
**3.2.1.1.Procedure 1 (P1): Preparation of Nanoparticles with the Surfactant 'Poly-L-L……**..... 22

**3.2.1.2.Procedure 2 (P2): Preparation of Nanoparticles with Surfactant 'Tween 80'**…….....23

**3.2.2.Preparation of Curcumin –loaded Alginate Nanoparticles (AA-Cur-NPs)**..... 24

**3.2.3.Preparation of Curcumin-loaded Chitosan-coated Alginate Nanoparticles (CS(AA-Cur-NPs))**..... 25

**3.2.4.Conjugation of Folic Acid (FA) on the Surface of Nanoparticles (FA-CS(AA-CurNPs)**……..…….....26

**3.2.5.Characterization of FA conjugated Nanoparticles** ..... 26

**3.2.5.1.Stability Study for Nanoparticles** ..... 28

**3.2.6.Drug Release Profiles of Functionalized Nanoparticles** ..... 28

**3.2.7.Preparation of Nanoparticle-Embedded Hydrogel Scaffolds (HG/CS(AA_NPs))** ..... 29

**3.2.8.Characterization of Nanoparticle-Embedded Hydrogel Scaffolds**..... 30

**3.2.8.1.Rheological Test of Nanoparticle-Embedded Hydrogel Scaffolds**..... 30

**3.2.8.2.Thermo-responsiveness of Nanoparticle-Embedded Hydrogel Scaffolds**…….30

**3.2.8.3.Swelling Capacity of Nanoparticle-Embedded Hydrogel Scaffolds**..... 31

**3.2.9.Drug Release Studies of Nanoparticle-Embedded Hydrogel Scaffolds**... 31

**4.RESULTS** ..... 33

**4.1.Preparation of Drug Delivery System** ..... 33

**4.1.1.Preparation of Alginate Nanoparticles (AA-NPs)**..... 33

**4.1.2.Preparation of Curcumin-loaded Chitosan-coated Alginate Nanoparticles (CS(AA-Cur-NPs))** ..... 36

**4.1.3.Functionalization of the Nanoparticle Surface with Folic Acid (FA)**..... 39

**4.1.4.Characterization of Functionalized Nanoparticles** ..... 40

**4.2.Preparation of Nanoparticle-Embedded Hydrogel Scaffolds (HG/CS(AA-Cur_NPs))** ..... 47

**4.2.1.Characterization of Nanoparticle-Embedded Hydrogel Scaffolds**..... 47

**4.2.1.1.Rheological Test of Nanoparticle-Embedded Hydrogel Scaffolds**..... 48

**4.2.1.2.Thermo-responsiveness of Nanoparticle-Embedded Hydrogel Scaffolds**…….51

**4.2.1.3.Swelling Capacity of Nanoparticle-Embedded Hydrogel Scaffolds**..... 53

**4.3.Drug Release Profiles of Nanoparticles and Nanoparticle-Embedded Hydrogel Scaffolds** ..... 54

**5.DISCUSSION** ..... 57

**6.CONCLUSION**..... 72

**7.REFERENCES**..... 74

**8.APPENDICES** ..... 78

**9.CURRICULUM VITAE**..... 86

# ACKNOWLEDGMENT

Firstly, I would first like to express my deep and sincere gratitude to my research supervisor, Assist. Prof. Özgül Gök for her patience, motivation and enthusiasm. Her guidance has greatly helped me to perform this research and writing of this thesis.

I am grateful to my friends always supporting me; İrem Soyhan, Gizem Canko, Ali Murad Özmen, İleyna Üvak, Rabia Güner, Bercis İlik.

Finally, I must express my very profound gratitude to my parents (Mehmet Ertuğral and Güler Ertuğral) and to my brother (Hasan Eren Ertuğral) for providing me with unfailing support and continuous encouragement throughout my education life.

This research has been supported by Acibadem Mehmet Ali Aydinlar University Scientific Research Commission (ABAPKO Project No: 2019/04-04).

## LIST OF ABBREVIATIONS

| | |
|---|---|
| AA | Alginate |
| $C_E$ | Effective Concentration |
| $C_I$ | Ineffective Concentration |
| $C_T$ | Toxic Concentration |
| CS | Chitosan |
| Cur | Curcumin |
| DDS | Drug Delivery System |
| FA | Folic Acid |
| HG | Hydrogel |
| NP | Nanoparticle |
| P1 | Procedure 1 |
| P2 | Procedure 2 |

# LIST OF FIGURES

**Figure 1.** Preparation of drug-loaded nanoparticle incorporated injectable hydrogel based drug delivery system ..... 6

**Figure 2.** Comparison of drug concentrations in systemic circulation resulting from administration of a drug by intravenous. CT, toxic concentration; CE effective concentration; CI, ineffective concentration ..... 7

**Figure 3.** Crosslinking of sodium alginate with cationic calcium chloride ..... 11

**Figure 4.** Surface modification of nanoparticles ..... 12

**Figure 5.** Structural organization of biodegradable drug-loaded nanoparticles ..... 14

**Figure 6.** Hydrogel preparation scheme ..... 16

**Figure 7.** Stimuli-response hydrogel ..... 17

**Figure 8.** Thermo-responsive hydrogel mechanism ..... 18

**Figure 9.** Thermo-responsive polymers ..... 19

**Figure 10.** Comparison of prepared alginate nanoparticles with different calcium chloride concentrations ..... 33

**Figure 11.** Effect of different amount of surfactant and different temperature on preparation of alginate nanoparticles ..... 34

**Figure 12.** Zeta potential graphs of (A) control NP in P1 and (B) chitosan-coated control NP in P1 ..... 36

**Figure 13.** Zeta potential graphs of (A) drug-loaded NP in P1 and (B) chitosan-coated drug-loaded NP in P1 ..... 37

**Figure 14.** Zeta potential graphs of (A) control NP in P2 and (B) chitosan-coated control NP in P2 ..... 37

**Figure 15.** Zeta potential graphs of (A) drug-loaded NP in P2 and (B) chitosan-coated drug-loaded NP in P2 ..... 38

**Figure 16.** FTIR spectra of (A) FA conjugated P1 nanoparticles and (B) FA conjugated P2 nanoparticles ..... 39

**Figure 17.** Size determination of P1 nanoparticles with Dynamic Light Scattering. (A) Drug-loaded NP in P1 (B) Control NP in P1 (C) Chitosan-coated drug-loaded NP in P1 (D) Chitosan-coated control NP in P1 ..... 40

**Figure 18.** Size determination of P2 nanoparticles with Dynamic Light Scattering. (A) Drug-loaded NP in P2 (B) Control NP in P2 (C) Chitosan-coated drug-loaded NP in P2 (D) Chitosan-coated control NP in P2 ..... 41

**Figure 19.** Size determination of FA conjugated nanoparticles with Dynamic Light Scattering. (A) FA conjugated NP in P1 (B) FA conjugated NP in P2 ..... 41

**Figure 20.** Stability Test of (A) Control NP in P1 (B) Control Np in P2 (C) Chitosan-coated control NP in P1 (D) Chitosan-coated control NP in P2 ..... 42

**Figure 21.** Stability Test of (A) Drug-loaded NP in P1 (B) Drug-loaded NP in P2 (C) Chitosan-coated drug-loaded NP in P1 (D) Chitosan-coated drug-loaded NP in P2 ..... 42

**Figure 22.** Stability Test of (A) FA conjugated NP in P1 (B) FA conjugated NP in P2 ..... 43

**Figure 23.** Morphological evaluation of P1 nanoparticles with Transmission Electron Microscopy. (A) Control NP in P1 (B) Drug-loaded NP in P1 (C) Chitosan-coated control NP in P1 (D) Chitosan-coated drug-loaded NP in P1 ..... 44

**Figure 24.** Morphological evaluation of P2 nanoparticles with Transmission Electron Microscopy. (A) Control NP in P2 (B) Drug-loaded NP in P2 (C) Chitosan-coated control NP in P2 (D) Chitosan-coated drug-loaded NP in P2 ..... 45

**Figure 25.** Micelle formation in Procedure 2 ..... 46

**Figure 26.** Morphological evaluation of FA conjugated nanoparticles with Transmission Electron Microscopy. (A) FA conjugated nanoparticles with in P1 (B) FA conjugated nanoparticles with in P2 ..... 46

**Figure 27.** Morphological evaluation of control PNIPAM hydrogel scaffolds with Scanning Electron Microscopy. (A) dry (B) wet ..... 47

**Figure 28.** Morphological evaluation of pNIPAm hydrogel scaffolds with Scanning Electron Microscopy. (A) P1-NP incorporated pNIPAM hydrogel scaffold (B) P2-NP incorporated pNIPAM hydrogel scaffol ..... 47

**Figure 29.** Degradation evaluation of pNIPAM hydrogel scaffolds with rheometer. (A) Control pNIPAM hydrogel scaffolds (B) P1-NP incorporated pNIPAM hydrogel scaffolds (C) P2-NP incorporated pNIPAM hydrogel scaffolds ..... 48

**Figure 30.** Gelation evaluation of control hydrogel scaffolds with rheometer. (A) 0.1 Hz (B) 50.5 Hz (C) 100 Hz ..... 49

**Figure 31.** Gelation evaluation of P1 nanoparticles incorporated pNIPAM hydrogel scaffolds with rheometer. (A) 0.1 Hz (B) 50.5 Hz (C) 100 Hz ..... 50

**Figure 32.** Gelation evaluation of P5 nanoparticles incorporated pNIPAM hydrogel scaffolds with rheometer. (A) 0.1 Hz (B) 50.5 Hz (C) 100 Hz ..... 50

**Figure 33.** Scratch before the injection (A) and after the injection (B) of thermo-responsive pNIPAM polymer mixture ..... 51

**Figure 34.** After the injection of thermo-responsive pNIPAM hydrogel mixture (A) P1-NP incorporated (B) P2-NP incorporated ..... 51

**Figure 35.** Degradation of pNIPAM hydrogel scaffold into tissue sample ..... 52

**Figure 36.** Swelling capacity profiles of (A) control hydrogel scaffold (B) P1 nanoparticles incorporated pNIPAM hydrogel scaffold (C) P1 nanoparticles incorporated pNIPAM hydrogel scaffold ..... 53

**Figure 37.** Calibration Curve for Curcumin drug molecule drawn by the intensity of mass peak of molecular ion with m/z ratio as 365.2 ..... 54

**Figure 38.** Drug release profiles from nanoparticles prepared by Procedure 1 and nanoparticle-embedded hydrogels ..... 55

**Figure 39.** Drug release profiles from nanoparticles prepared by Procedure 2 and nanoparticle-embedded hydrogels ..... 56

**Figure 40.** Design of the drug-loaded and ovarian cell targeted nanoparticle and its encapsulation into a thermoresponsive and injectable hydrogel scaffold ..... 57

**Figure 41.** Degredation evaluation of control pNIPAM hydrogel scaffolds with rheometer ..... 78

**Figure 42.** Degredation evaluation of P1 incorporated pNIPAM hydrogel scaffolds with rheometer ..... 79

**Figure 43.** Degradation evaluation of P2 incorporated pNIPAM hydrogel scaffolds with rheometer ..... 80

# LIST OF TABLES

**Table 1.** Effect of different amount of surfactant and different temperature on preparation of alginate nanoparticles in Procedure1 ..... 35

**Table 2.** Effect of different amounts of surfactant and different temperature on preparation of alginate nanoparticles in Procedure2 ..... 35

**Table 3.** Swelling capacity profiles of control hydrogel scaffold ..... 81

**Table 4.** Swelling capacity profiles of P1 nanoparticles incorporated pNIPAM hydrogel scaffold..... 82

**Table 5.** Swelling capacity profiles of P2 nanoparticles incorporated pNIPAM hydrogel scaffold..... 84

## SUMMARY

In this thesis, a drug delivery system that will allow the therapeutic substances to be administered to a specific part of the body in a minimally invasive way was prepared. For this purpose, a biomaterial-based platform has been designed that can release the anti-inflammatory drug active ingredient it contains by injecting it into the damaged tissue after ovarian surgery. Thanks to this system, it is foreseen that it will be possible to increase the concentration of the relevant active substances locally in the application area and to create a reserve that can release active substance slowly and continuously depending on time. In addition, thanks to the targeting molecule planned to be conjugated to nanoparticles, it is aimed to release the drug active substance in the ovarian cells where it is selectively targeted and show its effect. For this purpose, drug-loaded sodium alginate-based nanoparticles were prepared to provide slow, controlled and continuous release of the confined drug molecules. It was encapsulated or embedded in a heat sensitive polymeric hydrogel for ease of application and slowing down the rate of biodegradation. It is aimed to increase the stability and functionalization of sodium alginate-based nanoparticles, which are planned to be cross-linked with calcium chloride and have a high drug carrying capacity, by coating them with chitosan natural polymer. The folic acid group was conjugated to the surface of nanoparticles coated with chitosan polymer to provide targeting properties to ovarian cells. Curcumin, an anti-inflammatory drug with a well-known mechanism of action, was entrapped into the hydrophilic core of the nanoparticles. The prepared drug loaded nanoparticles will be mixed with the heat sensitive polymer pNIPAM chains and will be confined within the hydrogel structure that these polymer chains will form. Thus, this drug delivery system was able to provide a treatment method that allows the entrapped drug active substance to act on target cells selectively and with slow and sustained release locally. Thus, the potential of nanoparticles, which are both biocompatible and biodegradable, loaded with curcumin anti-inflammatory drugs and specifically targeted to ovarian cells, as a drug delivery system were investigated.

**Keywords :** Anti-inflammatory, Curcumin, Drug Delivery Systems, Injectable Hydrogels, Thermo-sensitive Hydrogels

# ÖZET


**İlaç Yüklü Nanoparçacıkların Hazırlanması ve Termoduyarlı Hidrojeller İçerisine Hapsedilerek Enjekte Edilebilir İlaç Taşıma Sistemlerin Geliştirilmesi**

Önerilen tez kapsamında, vücudun belirli bir bölgesine minimal invaziv bir yolla terapötik özelliği olan maddelerin uygulanmasını sağlayacak bir ilaç taşıma sistemi hazırlanmıştır. Bu amaçla, yumurtalık ameliyatları sonrasında hasar gören dokuya enjekte edilerek içerdiği anti-inflamatuar ilaç etken maddesini kontrollü olarak salabilecek biyomalzeme bazlı bir platform tasarlanmıştır. Bu sistem sayesinde uygulama bölgesinde lokal olarak ilgili etken maddelerin konsantrasyonunu arttırmanın ve zamana bağlı olarak yavaş yavaş ve sürekli etken madde salımı yapabilen bir rezervin oluşturulmasının mümkün olabileceği öngörülmektedir. Ayrıca nanoparçacıklara konjüge edilmesi planlanan hedefleyici molekül sayesinde ilaç etken maddesinin seçici olarak hedeflendirildiği yumurtalık hücrelerinde salınması ve etkisini göstermesi hedeflenmiştir. Bu amaçla, hapsedilen ilaç moleküllerinin yavaş, kontrollü ve sürekli salımını sağlamak için ilaç yüklü sodyum aljinat bazlı nanoparçacıklar hazırlanacak; uygulama kolaylığı ve biyobozunma hızını yavaşlatması adına ısıya karşı duyarlı bir polimerik hidrojel içine hapsedilmiştir. Kalsiyum klorit ile çapraz bağlanacak ve ilaç taşıma kapasitesi yüksek olacak şekilde hazırlanması planlanan sodyum aljinat bazlı nanoparçacıkların kitosan doğal polimeri ile kaplanarak kararlılığının arttırılması ve fonksiyonelleştirilmesi gerçekleştirilmiştir. Tasarlanan çapraz bağlı yapı sodyum aljinat-kalsiyum klorit redoks reaksiyonu sonucu elde edilmiştir. Folik asit grubu, kitosan polimeri ile kaplanmış nanoparçacıkların yüzeyine konjüge edilerek yumurtalık hücrelerini hedefleyici özellik sunabilecektir. Nanoparçacıkların hidrofilik çekirdeğine oldukça sık kullanılan ve etki mekanizması iyi bilinen bir anti-inflamatuar ilaç olan kürkümin yüklenmiştir. Hazırlanan ilaç yüklü nanoparçacıklar, ısıya duyarlı polimer pNIPAM zincirleri ile karıştırılarak bu polimer zincirlerinin oluşturacağı hidrojel yapının içine hapsedilmiştir. Böylelikle önerilen bu ilaç taşıma sistemi, hapsedilen ilaç etken maddesinin lokal olarak yavaş ve sürekli

salımıyla ve de seçici olarak hedef hücrelerde etki göstermesini sağlayabilecek bir tedavi yöntemi sunabilecektir.

**Anahtar sözcükler :** Anti-inflamatuvar, Enjekte Edilebilir Hidrojeller, İlaç Taşıma Sistemleri, Kurkumin, Termoduyarlı Hidrojeller

# 1. BACKGROUND AND AIM OF THE STUDY

The aim of this project is to develop a minimally invasive drug delivery system that is targeted only to ovarian cells and has the potential to eliminate inflammation in the operated area after any surgical intervention in the ovaries and reduce ovarian cell loss/damage.

Within the scope of the project, it is achieved to prepare biodegradable and biocompatible nanoparticles that may act selectively on target cells and to provide slow and controlled release of drug molecules to be applied in treatment. Later on, these nanoparticles were confined within the injectable hydrogel structure prepared with a heat sensitive polymeric biomaterial for ease of application and slowing down the biodegradation rate. This drug delivery system allows for the combined use of targeted drug delivery and three-dimensional scaffold structures for both local application of biomaterials and delivery of therapeutic agent in a controlled and sustained manner specifically in the targeted (and mostly exposed to inflammation) ovarian cells. In addition, since no examples of this polymer-drug combination have been found in the literature, this novel design of nanoparticle-hydrogel system can be evaluated as an advantageous injectable platform with high potential in both improving wound healing and diminishing anti-inflammatory effects in case of surgery or internal tissue damage.

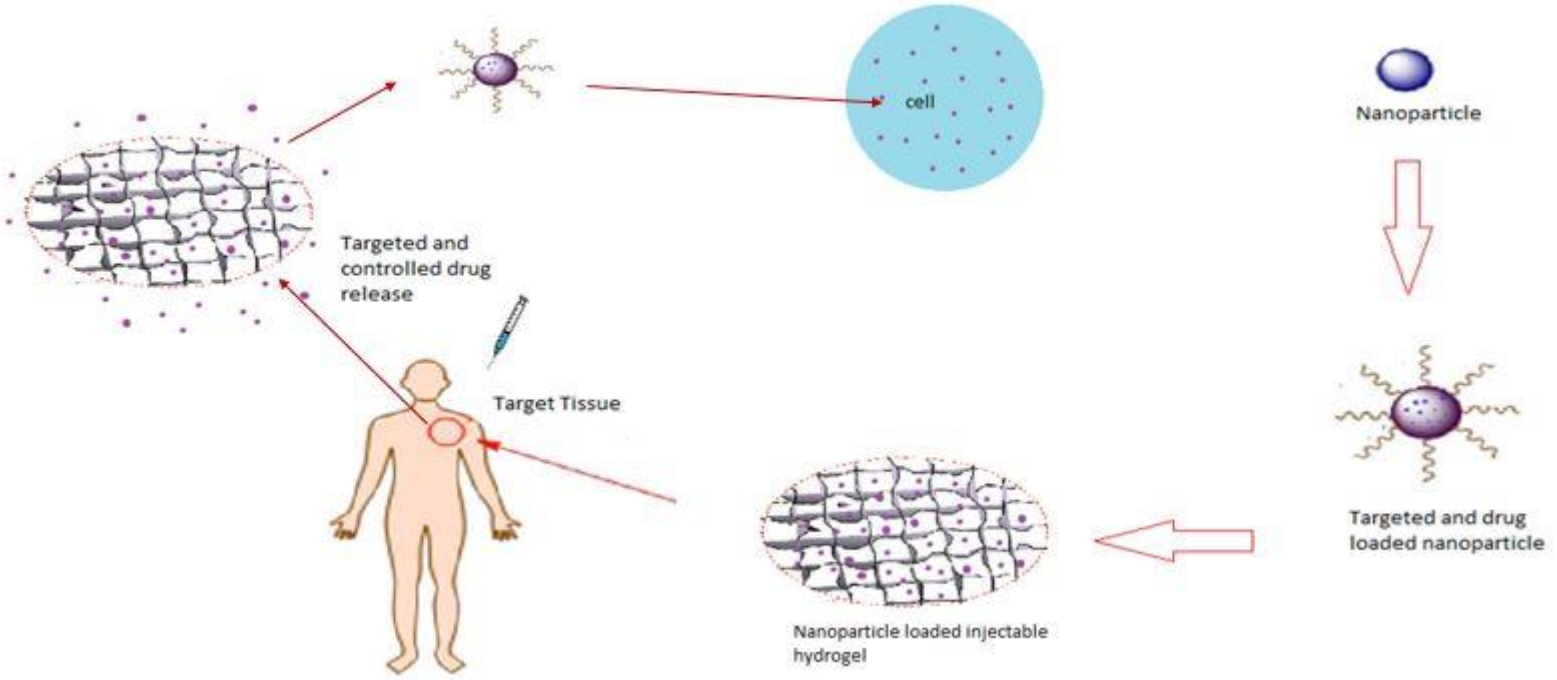


**Figure 1.** Preparation of drug-loaded nanoparticle incorporated injectable hydrogel based drug delivery system

# 2. INTRODUCTION

## 2.1. Drug Delivery Systems (DDSs)

Recently, it has been figured out that pharmacokinetic factors have a crucial role on therapeutic effects and undesirable actions of drugs. Therefore, scientists have been aware of the importance of studies on drug metabolism and disposition. This growing awareness has shown that therapeutic effect is not sufficient only by the administration of a drug but also depends on appropriate concentration of drug for a certain duration on a particular target site. Since the route of administration of a drug can has undesirable actions, concentration of administered drug should have been kept in control (1). Because, even if the drug is injected into the systemic circulation directly, administered dosage and drug level at the target site will not be coherent (2).

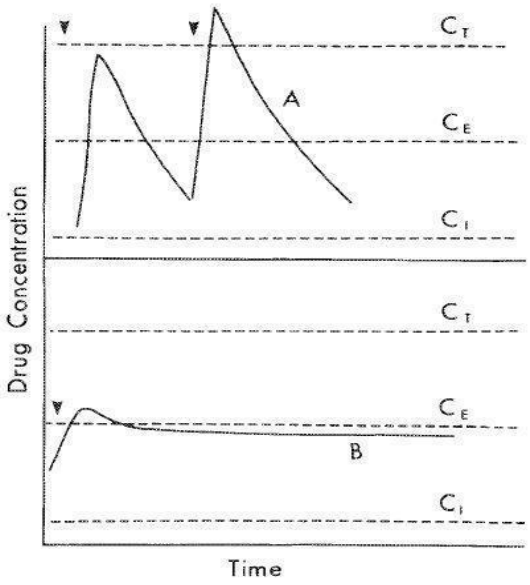


**Figure 2.** Comparison of drug concentrations in systemic circulation resulting from administration of a drug by intravenous. CT, toxic concentration; CE effective concentration; CI, ineffective concentration (2)

In *Figure 1*, comparison of drug concentrations in systemic circulation after administration of a drug and toxic ($C_T$), effective ($C_E$) and ineffective ($C_I$) drug concentration are demonstrated. When a drug is injected into systemic circulation, drug concentration typically rises rapidly and declines by first-order exponential decay and drug concentration oscillate around effective ($C_E$) and ineffective ($C_I$) concentration, even it reaches the toxic ($C_T$) concentration (curve A). With this type of drug concentration oscillations where the therapeutic index ($C_T/C_E$) is low, ineffective therapeutic actions with undesirable side effects are inevitable. Curve B illustrates the required drug concentration levels after administration of a drug, constant (zero-order release) release of a drug into systemic circulation. It is possible to achieve desired therapeutic effect with maintained release rate (2).

Other incoherence between administered dose and drug levels has been attributed also poor activity in vivo. Poor activity is the term 'bioavailability' of drugs, the extend and rate which drug reaches and shows effect in target tissue. When a drug is administered into the system, drug bioavailability is typically very low, and the concentration of the drug can quickly drop below an effective level, requiring re-administration. This led to undesirable side effects and more importantly toxicity (3).

It has become clear that beneficial therapeutic effects can be achieved by an appropriate administration formulation that can be controlled temporal and spatial aspects of drug disposition. This consideration has led the scientist drug delivery system concept (2). Drug delivery system (DDS) is the method or process of alternative approach for administering a pharmaceutical compound to regulate bioavailability and therapeutic effect. DDSs provide to control both routes of administered drug, drug metabolism, and the extend and rate of drug release at which drug reaches into the target site (4). DDS represents an attractive approach for controlled release of administered drug. Therefore, duration of action of drug can be extended, fluctuations of drug level in system and frequency of dosing can be reduced.

Besides, DDSs provide improvement drug utilization with maximizing availability with minimum dose, minimize or eliminate local and systemic side effects and drug accumulation (4)(5). In DDSs, polymeric network structure provide an alternative approach to administrate a therapeutic compound with incorporation (3). The demand to improve bioavailability of drugs and achieve appropriate therapeutic effect is to be satisfied with already existing biocompatible encapsulation materials (6)

### 2.1.1. Nanoparticles (NPs)

In drug delivery systems, various carriers with a wide range sized are used due to intended purpose. Nanoparticles, microspheres, implant surface coating, wafer etc. are the intensively used and advantageous carriers in drug delivery systems. Carrier is chosen for better encapsulation due to its grand bioavailability and less toxic properties. Polymeric nanoparticles, liposomes, dendrimers etc. are commonly used carriers due to their ability of controlled release and improvement of effectiveness of capsulated drugs.

Since the size and size distributions of carriers are important to determine their interaction with the cell membrane and their penetration across the barriers, nano-sized carriers are commonly preferred. These nano-sized carriers, “nanoparticles”, are preferred due to their small size, customizable surface, improved solubility, and multi-functionality and designed for target, diagnose and treatment. Nanoparticles are vary in size from 10 to 1000 nm but less than 200 nm sized nanoparticles are preferred for prolonged blood circulation and easy administration (7). Various hydrophilic/ hydrophobic therapeutic molecules and drugs are improved by using biodegradable nanoparticles to improve solubility and circulation time. Therefore, therapeutic index of drug, specificity, tolerability and drug efficacy increases by nanoencapsulation of drugs (nanomedicine) and this reduces risk of toxicity and patient expences. Besides,

using nanoparticle increases interaction with the biological environment by enhancing absorption into selected tissue (8).

#### 2.1.1.1. Polymeric Nanoparticles

Depending on the method of preparation, possessed different properties and release characteristics natural and synthetic polymers are used for synthesis of nanoparticles according to application purpose and type of drug/therapeutic molecule to be encapsulated. Biodegradable nanoparticles are commonly formulated from PLA, PLGA, PCL etc. type synthetic polymers for effective targeting (9). Specially biocompatible natural polymers such as alginate, chitosan, gelatin etc. are preferred because they can easily extracted from natural resources and are cost effective (10).
Alginate is a water soluble linear polysaccharide which is composed of differently arranged blocks of 1-4 linked α-L-guluronic and β-D-mannuronic acid residues and extracted from black sea weed and brown algae (10). Alginate has been widely used in drug delivery systems and cell encapsulation as it is biocompatible, biodegradable and mucoadhesive (11). It has easy gelling property by addition of a polycationic solution and micro and/or nanoparticle can be formed easily by inducing with calcium ions (*Figure 2*) (12). Alginate based nanoparticles can transform hydrophobic molecules like curcumin dispersible in aqueous media and eliminate the deficiency of poor solubility of hydrophobic molecules (13).

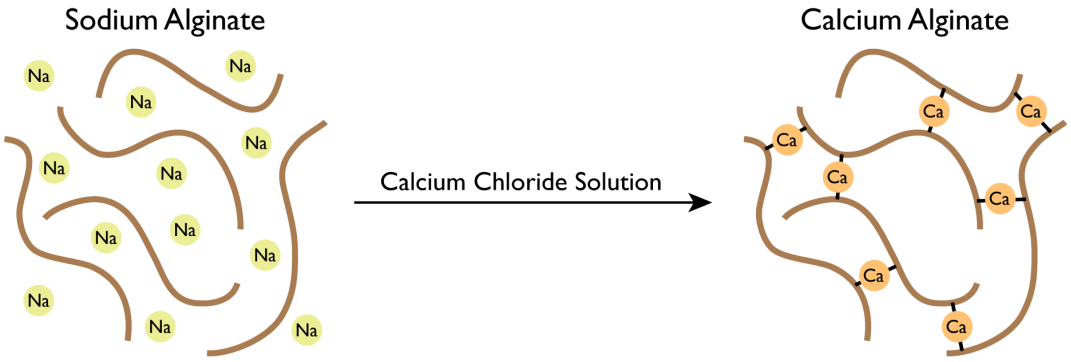


**Figure 3.** Crosslinking of sodium alginate with cationic calcium chloride

As an alternative, chitosan is another linear polysaccharide, a derivative of chitin; partially deacetylated polymer of N-acetylglucosamine and mostly protonated at pH<6.5, thus in these conditions it possessed polycation property (10). Despite of insoluble in water and organic solvent unlike alginate, chitosan is soluble in dilute acid solution. Chitosan and its derivatives are known as biodegradability, bioavailability and non-toxic properties and have been widely used in drug delivery systems (14).

### 2.1.2 Targeted Nanoparticles

Small size and use of biodegradable polymers are the advantages of using nanoparticles in drug delivery systems. These advantages allow nanoparticles easy circulation in bloodstream and efficient uptake by various cell types and drug accumulation at target sites. For successful and efficient advantage of nanoparticles, persistence of nanoparticles is required in systemic circulation of the body. In despite of formulation nanoparticles with hydrophilic characteristic or coating the nanoparticles with hydrophilic polymers/surfactants are alternative approach for minimizing opsonization and prolong the circulation time, modification/conjugation

of surface of nanoparticles with therapeutic agent or cell-specific ligand is required for active targeting (*Figure 3*.) (8)(9)(15).

To achieve sustained systemic circulation of nanoparticles surface of nanoparticles must be modified to prevent phagocytosis (8). Increase the site-specific targeting tissue specific of nanoparticle must be increased. Small non-antigenic ligands have been commonly started to use due to their advantages (5).

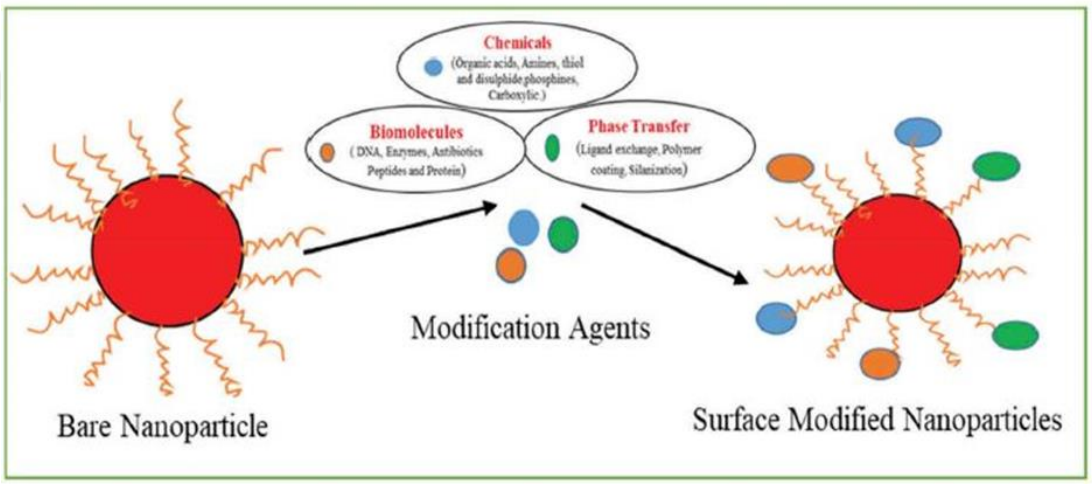


**Figure 4.** Surface modification of nanoparticles (16)

Folic acid (FA) is one of the most popular ligand presents advantages as a targeting agent as stable, inexpensive, and non-immunogenic compared with proteins and has high affinity for its cell receptor, folate receptor (14). It has been found that during inflammation, folate receptors are strongly upregulated on activated macrophages. Therefore, design of active targeting drug delivery system with folic acid modified nanoparticles for targeting activated macrophages is an attractive approach for inflammation treatment (17).

### 2.1.3. Functionalization

Since alginate nanoparticles are obtained with crosslinking of the alginate polymer by electrostatic interaction with calcium ions, polymer forms a matrix capable of entrap drugs. Besides, alginate polymer tends to form a polyelectrolyte complex with cationic polymers such as chitosan. Association between the acid group of alginate and the amine group of chitosan provides polyelectrolyte complex coating. In *2011, Cook et. al.* have been suggested that coating the alginate nanoparticles with chitosan might be improved the mechanical strength of alginate nanoparticles (18).

On the other hand, while coating the nanoparticles with chitosan provides positive surface charge to improve functionalization of surface, also prolong the interaction time of encapsulated molecule with epithelium and enhance the absorption via the paracellular transport pathway through the tight junctions (10)(12). However, it has been figure out that functionalization of nanoparticles has many advantages besides extended interaction time. Recently, functional nanoparticles have been started to use for various biomedical and clinical applications for treatment, monitoring and targeting (19)(20). Although coating the nanoparticles with chitosan provides functionality for nanoparticles, chitosan polymer is not sufficient for the targeted administration but thanks to amine group of chitosan, functionalization capability can be improved by conjugates, specially conjugation of chemical or biological or targeting agents with NHS-ester bonds is an effective approach (21). In *2010, Huh et. al*. designed a chitosan/polyethylenimine nanoparticles with siRNA for tumor-homing to test imaging system for detection of RFP intensity (20). As another efficient example of functional nanoparticles for targeting is *J.Ji and his groups*, designed a MTX encapsulated FA conjugated chitosan nanoparticles to improve the tumor cell-selective targeting and induced the drug toxicity (21).

### 2.1.4. Drug Loading

In polymeric nanoparticles, high efficiency drug loading capacity has been expected and loading of interested drug can be accomplished by various ways such as dissolved, entrapped/encapsulated and adsorbed/attached into or onto a polymeric matrix (*Figure 4.*). Drug can be incorporated at the time of nanoparticle formation or drug can be attached after nanoparticle formation, incubating the nanoparticle into concentrated drug solution. Since entrapment of drug into polymeric nanoparticles has an advantage in terms of drug stability and sustained&slow drug release. Entrapment efficiency and drug loading depend on solubility of drug and polymer that is used for formulation of nanoparticle. Also, polymer composition, molecular weight, interaction between drug and polymer and the functional groups are effective on drug loading and entrapment efficiency (8)(9).

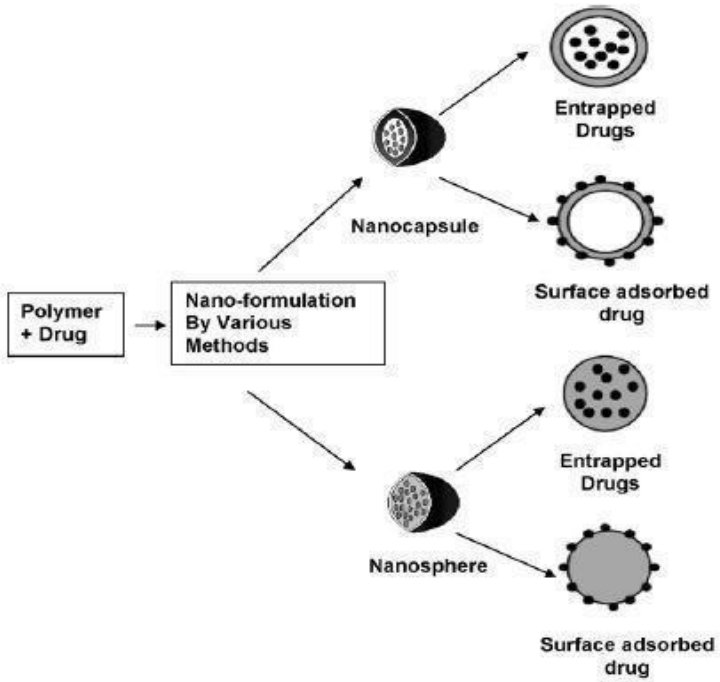


**Figure 5.** Structural organization of biodegradable drug-loaded nanoparticles (8)

In the last decade, it has been believed that medicinal plants are major source of therapeutic molecules in the traditional medicine to treatment and medicinal plants are healthier that synthetic ones. Curcumin is a one of the common spice known as active ingredient in turmeric and used for its medicinal and anti-inflammatory properties (22). Curcumin has been known to act as antioxidant, anti-mutagen and anti-carcinogenic and protective effect on reproductive organs activity (23). Since curcumin regulates the functioning of inflammatory enzymes, it can be employed for reduce post-operative inflammation (13)(24). Studies shows that formulated biodegradable polymeric carriers with curcumin for the treatment of inflammation in arthritic rats successfully employed for therapeutic management of inflammation (25). Despite curcumin is safe evet at high doses but its therapeutic effect is limited as it has poor aqueous solubility and rapid systemic elimination, which restrains its bioavailability (13). *Bisht et.al*. have been resolved this inefficiency by encapsulating curcumin in a polymeric nanoparticle, nanocurcumin, and provides an opportunity to expand the use of curcumin in clinical treatment (26). However, *Inchai et.al*. have showed in their study that curcumin solubility is proportional with the surfactant addition (27). The polysorbate 80 also known as tween 80 is a surfactant and nonionic emulsifier used as dispersing agent for nanoparticle synthesis (28). Since the surfactants play role in the formation of nanoparticles by lowering the interfacial tension, therefore they prevent particle aggregation (29). On the other hand, surfactants and other possible additives and agents such as cationic polymer poly-(l)-lysine, ease formulation of polymeric nanoparticles with different functional groups and improve stability (12).

### 2.1.5. Hydrogels

Local drug delivery systems have been intended to overcome shortcomings of conventional drug pharmacokinetic mechanisms. Since drug has to be delivered to response metabolic requirements, not only should matches temporal modulations also provide site-specific targeting. Such a system would be beneficial that delivered the therapeutic agent by some signal, sensed at the specific target and release the

therapeutic agent in response. This idea has led scientists to development of smart drug delivery systems (1).

Hydrogels have been started to use extensively for a wide variety of biomedical application. Hydrogels are three-dimensional cross-linked polymer networks which has high-water content that provides capability of swelling or de-swelling. In another word, polymerization of monomers either the presence of cross-linker and initiator depending on functional groups of polymer and cross-linker (*Figure 5*).

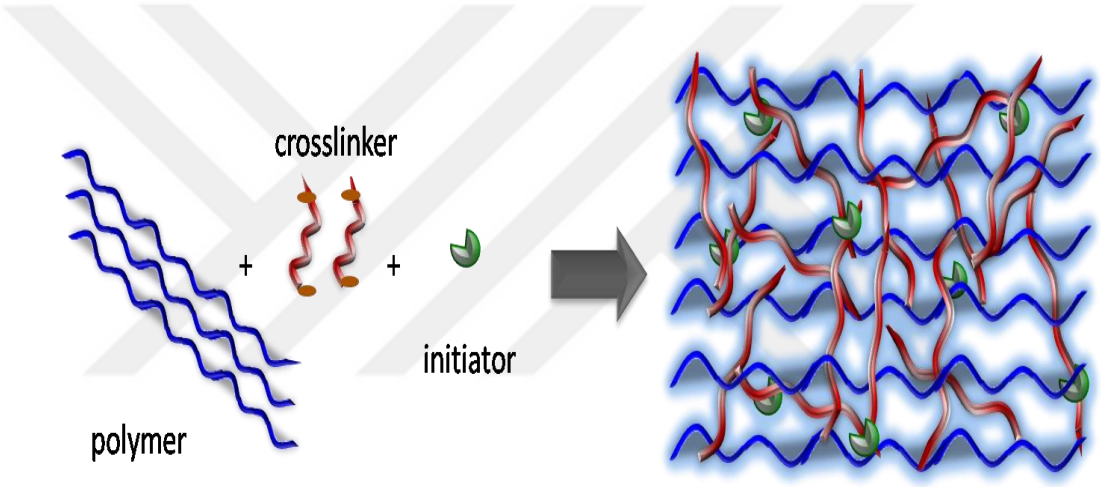


**Figure 6.** Hydrogel preparation scheme (adapted from (30))

Hydrogels are capable of retaining large volume in swollen state for sustained release of therapeutic agent. The ability of resistance to dissolution of hydrogels comes from the hydrophilic functional groups and molecular entanglements arises from cross-linking between polymeric chain networks. They can be classified as natural, synthetic and hybrid, as is the type of polymer that made of. Hydrogen bonding, ionic and hydrophobic interactions provide stabilization of hydrogels and hydrogels can be cross-linked by covalent bonds.

Thanks to the biocompatibility and biodegradability of polymers, development of in situ forming hydrogels has led smart drug delivery systems. Since the polymers that the scaffold material of hydrogels and polymerization/crosslinking methods are tunable, hydrogels can be designed as responds and changes with external environmental conditions. They can be designed that perform as stimulated by physical (temperature, electric or magnetic field etc.) or chemical (pH, ionic strength, solvent composition etc.) conditions (*Figure 6.*) and known as 'stimuli-responsive' hydrogels (3)(30)(31).

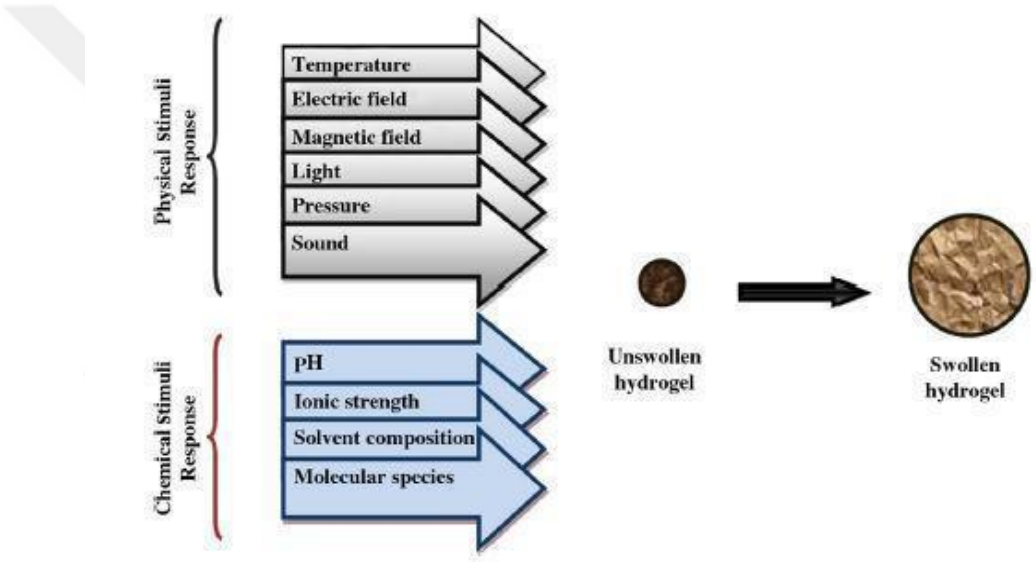


**Figure 7.** Stimuli-response hydrogel (30)

Thermo-responsive hydrogels are commonly known stimuli-responsive hydrogels and they have been extensively used in biomedical applications due to phase transition capability of polymers to change in external environment (*Figure 7*). The ability of gelation at physiological temperatures provides hydrogels to injectability and they can solidify to from gel in situ at body temperature in the desired tissue. Thermo-

responsive injectable hydrogels transform from a liquid to hydrogel at a threshold temperature which is defined as ‘lower critical solution temperature’ (LCST).

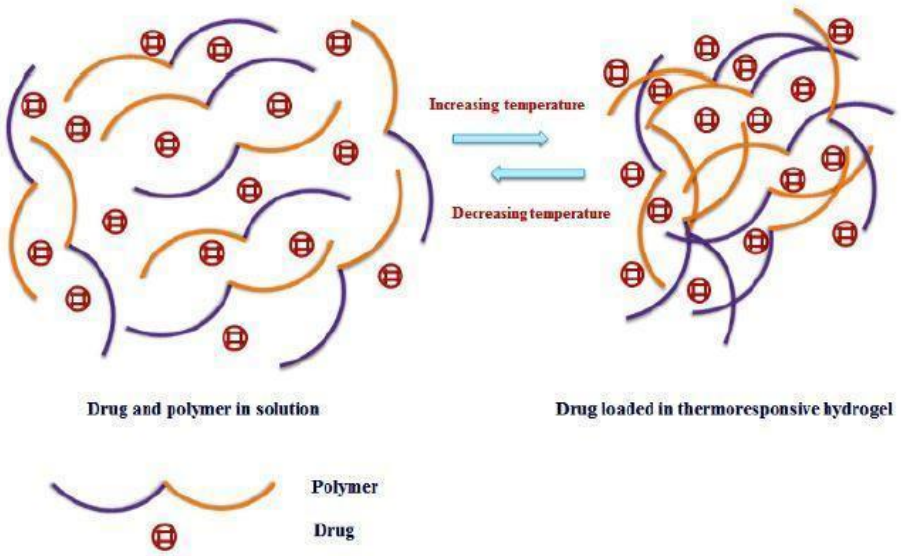


**Figure 8.** Thermo-responsive hydrogel mechanism (31)

To make thermo-responsive injectable hydrogels, thermo-responsive polymers such as poly(lactic-co-glycolic acid)–PEG, poly(N,N-diethylacrylamide), pNIPAM and poly(ethylene glycol-b-[DL-lactic acid-co-glycolic acid]-b-ethylene glycol) are needed (*Figure 8*). Thermo-responsive polymers can undergo phase transition without any chemicals and change physical properties with temperature. At low temperatures, while thermo-responsive polymers are liquid, they solidify with the increasing temperature and form semi-solid gel at high temperatures (32).

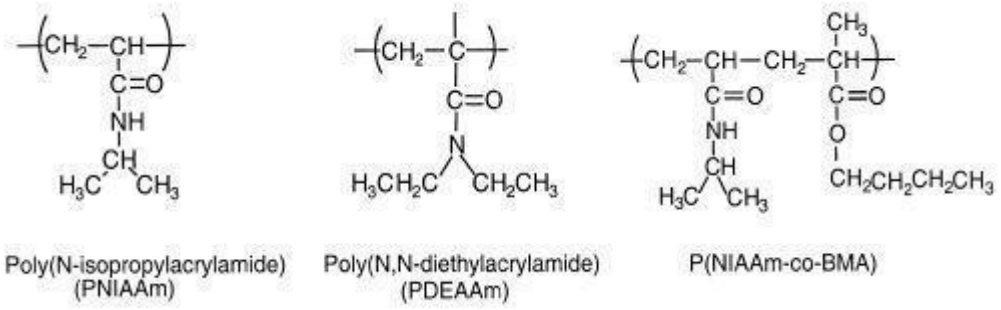


**Figure 9.** Thermo-responsive polymers (1)

Poly(N-isopropylacrylamide) (pNIPAM) is a polymer which is mostly preferred for preparing temperature- responsive hydrogels and widely examined and used in many other application areas. Microfluidic devices, cell culture substrates, drug delivery vehicles and soft actuators are some examples of these application areas. pNIPAM shows a broad and invertible volume change in water at its lower critical solution temperature (LCST, typically 32-35 °C) by virtue of coil-globule transition of the network strands of the polymer. At the temperatures under its LCST, pNIPAM molecules in an aqueous condition displays a hydrophilic act with an extended coil format, which continues with a water uptake and swelling. On the hand temperatures above the LCST, the hydrophobic groups starts to become highly more active, this leads to causing the molecules to convert into a shape resembling a compact globule (33)(34).

### 2.1.6. Nanoparticle Embedded Hydrogel Scaffolds as DDS

The injectability of thermo-responsive hydrogels has led to increment on relevance of use hydrogels in many applications. Recently, hydrogels have been used as dressing material for different types of wounds in wound healing process including inflammatory, remodeling or regeneration of damaged tissue. With the help of natural or synthetic biomaterials and their bioavailable characteristic properties, hydrogels has

been attracted to researchers due to tunable properties and applicability in site-specific target (35).

In situ application of thermo-responsive hydrogels provide assist for wound healing. Due to swelling/de-swelling property, prepare a hydrogel as therapeutic molecule release mechanism has a promising approach for wound healing, specially treatment of inflammation type complications. Since the drug release from a hydrogel is a function of time and based on rate-limiting step, controlled release profile of hydrogels can be categorized in three; as diffusion-controlled, swelling-controlled, or chemically-controlled. In diffusion-controlled release mechanisms, while diffusion of drug depends on the pore size (5-100 nm) of the hydrogel and significantly retarded in the swollen state, in swelling-controlled release mechanisms diffusion of drug is faster than swelling and it led to control release behavior (3).

Sustained and slow release of a drug using cross-linked hydrogel is not sufficient; incorporation of another release system is an alternative approach. Incorporated drug-loaded carriers (microspheres, nanoparticles or nanoemulsion etc.) into hydrogel network has a promising approach to overcome inefficacy of conventional wound healing processes with only administration of drug-loaded carrier or use of hydrogel-based healing mechanism by itself. In *2016, Verma et.al.* had an efficient strategy for accelerate wound healing process with using sericin/chitosan-capped silver nanoparticles incorporated hydrogel to reduce the risk of bacterial infection (35). Subsequently, in *200*5, *Zhang et. al*. were proposed another novel strategy which is thermo-responsive pNIPAM nanoparticle incorporated pNIPAM hydrogel that its swelling based on diffusion-control and they compared conventional pNIPAM hydrogel with nanoparticle incorporated pNIPAM hydrogel as shrinkage kinetics and observed faster shrinkage rate with the nanoparticle incorporated hydrogel (34).

# 3. MATERIALS AND METHODS

## 3.1. Materials

Alginic acid sodium salt from brown algae (low viscosity), calcium chloride, sodium dodecyl sulfate (SDS), chitosan (LMW, 50-190 kDa), curcumin (from Curcuma longa (Turmeric), powder) and Tween 80 (for synthesis) were purchased from Sigma Aldrich for the preparation of nanoparticle.

Poly(N-isopropylacrylamide),N,N,N',N'-Tetramethylethylenediamine (bioreagent, suitable for electrophoresis ~ 99%), triethylene glycol dimethacrylate (contains 80-120 ppm MEHQ as inhibitor, 95%), folic acid (≥ 97%), diisopropylamine (≥99.5%), N,N-Dimethylformamide (anhydrous, ≥ 99.8%), ammonium persulfate (APS) (for molecular biology, for electrophoresis ≥ 99.8%), poly-L-lysine (0.1% (w/v) in H2O)) were purchased from Sigma Aldrich for the preparation of hydrogel scaffold. Aluminium oxide (90 active basic (0.063-0.200 mm) (activity stage I) for column chromatography) was purchases from Merck and used as filter to remove inhibitor of triethylene glycol dimethacrylate.

Acetate buffer (pH 5.5) was prepared with acetone and acetic acid (Merck) into distilled water; phosphate saline buffer tablets (Biomatik Corporation) in distilled water, both solutions were used for determination of drug release profile experiments. HATU, diethyl ether, sodium sulfate (anhydrous for analysis) were purchased from Merck. Spectrum™ Spectra/Por™ 6 (Pre-wetted Standard RC Dialysis Tubing, 1kD MWCO) was purchased from Fischer Science for dialysis.

## 3.2. Preparation of Drug Delivery Systems

Drug delivery system designed in this thesis was prepared in two parts; curcumin-loaded chitosan-coated alginate nanoparticles (CS(AA-Cur-NPs)) and their encapsulation into PNIPAM based hydrogel scaffold (CS stands for chitosan polymer, AA stands for alginic acid polymer and Cur is curcumin drug molecule).

### 3.2.1. Preparation of Alginate Nanoparticles (AA-NPs)

Literature reveals several different methods for the preparation of nanoparticles from alginate polymer. However specifically two procedures were selected based on the evaluation of the obtained results for the nanoparticles in the associated scientific papers. Together with the modifications in the steps of the above-mentioned procedures, nanoparticles were prepared as follows.

#### 3.2.1.1. Procedure 1 (P1): Preparation of Nanoparticles with the Surfactant 'Poly-L-Lysine'

Preparation of blank (without drug) alginate nanoparticles was taken from literature (11)(36). Briefly, sodium alginate (low viscosity) (0.05 g, 0.231 mmol) was dissolved in 10 mL ultrapure (Milli-Q) water. On the other side, calcium chloride (0.05549 g, 0.0005 mmol) was dissolved in 10 mL ultrapure water. After the addition of Sodium dodecyl sulfate (SDS) (0.01g) solution prepared in 10 mL ultrapure water into the alginate solution, lastly $CaCl_2$ solution was added onto the mixture. Continuous stirring for 1 hour at room temperature was followed by the filtration of this reaction mixture through 0.22 μm cellulose acetate syringe filter.

3 mL poly-l-lysine (0.1% v/v) and 3 mL SDS solution (0.1% w/v) were added to 4.75 mL calcium chloride (50 mM) solution while calcium chloride was being stirred. 0.25 mL sodium alginate solution (0.5% w/v) was added dropwise through by micropipette

and the mixture was mixed by stirring magnetically at 1500 rpm for 2 hours at 40 ºC in order to obtain nanoparticles. After 2 hours, the mixture was centrifuged at 14000 rpm for 30 min and rinsed with ultrapure water, centrifuged at 5000 rpm for 5 min. Washing step was repeated two times. Supernatant was decanted and filtered with 0.22 µm cellulose acetate syringe filter for further measurements for the characterization of prepared nanoparticles.

#### 3.2.1.2. Procedure 2 (P2): Preparation of Nanoparticles with Surfactant 'Tween 80'

Preparation of blank ( without drug) alginate nanoparticles was taken from literature (37). Briefly, sodium alginate (0.1g, 0.468 mmol) was dissolved in 10 mL ultra pure water. 0.1% (w/v) calcium chloride solution was prepared by dissolving 0.01 g calcium chloride in 10 mL ultra pure water. 1% (v/v) tween 80 solution was prepared by dissolving 0.1 mL in 10 mL ultra pure water. While calcium chloride and sodium alginate solutions were mixed by stirring magnetically for 1 hour without temperature, tween 80 solution was mixed by stirring only for 15 min to prevent micelle formation. All solutions were filtered with 0.22 µm cellulose acetate syringe filter, again except tween 80 solution.

6 mL of tween 80 (1% v/v) solution was added into 5 mL sodium alginate solution (0.1% w/v) and mixed by stirring for 15 min. 1 mL was taken from the mixture in order to make total volume 10 mL. Then 5 mL calcium chloride (0.1% w/v) was added dropwise through by micropipette while the tween 80 and sodium alginate mixture was stirring magnetically, and mixture was allowed to stir for 1 hour at 1500 rpm. After 1 hour, the mixture was centrifuged at 14000 rpm for 30 min and rinsed with ultrapure water, centrifuged at 5000 rpm for 5 min. Washing step was repeated two times. Supernatant was decanted and filtered with 0.22 µm cellulose acetate syringe filter for further measurements.

### 3.2.2. Preparation of Curcumin –loaded Alginate Nanoparticles (AA-Cur-NPs)

In Procedure 1, curcumin-loaded alginate nanoparticles were prepared with similar procedure with blank (without drug) nanoparticles. However, with the difference of addition of curcumin powder dissolved in ethanol (99%) solvent. Briefly, 10 mg curcumin powder was dissolved in 10 mL ethanol solvent. 9 µL curcumin solution was added in 4.75 mL calcium chloride (50 mM) solution while calcium chloride was being stirred. 3 mL poly-l-lysine (0.1% v/v) and 3 mL SDS solution (0.1% w/v) were added to mixture. 0.25 mL sodium alginate solution (0.5% w/v) was added dropwise by micropipette and the mixture was stirred at 1500 rpm for 2 hours in order to obtain nanoparticles. After 2h, the mixture was centrifuged at 14000 rpm for 30 min and rinsed with ultrapure water, centrifuged at 5000 rpm for 5 min. Washing step was repeated two times. Supernatant was decanted and filtered with 0.22 µm cellulose acetate syringe filter for further measurements.

In Procedure 2, curcumin-loaded alginate nanoparticles were prepared with similar procedure with blank (without drug) nanoparticles but with the difference of addition of curcumin powder directly. Briefly, 6 mL tween 80 (1% v/v) solution was added into 5 mL sodium alginate solution (0.1% w/v) and stirred magnetically for 15 min. Then 1.5 mg curcumin was added and stirred until dissolved properly. 5 mL calcium chloride solution (50 mM) was added dropwise through by micropipette while the mixture was stirring magnetically and mixture was allowed to stir for 1 hour at 1500 rpm. After 1 hour, the mixture was centrifuged at 14000 rpm for 30 min and rinsed with ultrapure water, centrifuged at 5000 rpm for 5 min. Washing step was repeated two times. Supernatant was decanted and filtered with 0.22 µm cellulose acetate syringe filter for further measurements.

### 3.2.3. Preparation of Curcumin-loaded Chitosan-coated Alginate Nanoparticles (CS(AA-Cur-NPs))

In this step, both blank (without drug) and curcumin-loaded (with drug) nanoparticles were coated with chitosan polymer. Both nanoparticles prepared by Procedure 1 and 2 were utilized for chitosan coating step.

Procedure for the coating of alginate-based nanoparticles with chitosan polymer was followed by literature example (9) with slight modifications. Briefly, chitosan (0.01g) (LMW) was dissolved in 10 mL ultrapure water for preparing 0.1% (w/v) chitosan solution. While chitosan solution was being stirred at 1500 rpm, blank (without drug) nanoparticles were added dropwise by micropipette with the ratio of Chitosan to Nanoparticle (C:NP) as 1:2 by volume/volume. Mixture was allowed to stir magnetically at 1500 rpm for 2 hours. After 2 hours, the mixture was centrifuged at 14000 rpm for 30 min and rinsed with ultrapure water, centrifuged at 5000 rpm for 5 min. Washing step was repeated two times. Supernatant was decanted and filtered with 0.22 μm cellulose acetate syringe filter for further measurements.

Above-mentioned procedure was followed for the coating of curcumin-loaded alginate nanoparticles. Briefly, as chitosan solution was being stirred at 1500 rpm, curcumin-loaded nanoparticles were added dropwise by micropipette with the ratio of 1:2 (C:NP). Mixture was allowed to stir at 1500 rpm for 2 hours. After 2 hours, the mixture was centrifuged at 14000 rpm for 30 min and rinsed with ultrapure water, centrifuged at 5000 rpm for 5 min. Washing step was repeated two times. Supernatant was decanted and filtered with 0.22μm cellulose acetate syringe filter for measurements.

### 3.2.4. Conjugation of Folic Acid (FA) on the Surface of Nanoparticles (FA-CS(AA-Cur-NPs)

FA-NP conjugate synthesis was done by following the literature (10). 1 mL of nanoparticle solutions (obtained by both P1 and P2) were lyophilized separately in 10 ml round-bottom flasks in order to perform FA-conjugation reaction. 3.9 mg HATU and 4.1 mg FA was added into lyophilized nanoparticles and round-bottom was closed with rubber septum. Inert condition was provided with nitrogen gas ($N_2$) with the help of needle through rubber septum. 0.68 µL DIPA and 1.5 mL anhydrous DMF solution wad added into round-bottom with syringe through rubber septum. Obtained mixture was stirred magnetically overnight in the dark to allow the conjugation reaction to occur.

Next day, dialysis was performed in order to remove free FA molecules and excess DMF in the solution. Briefly, FA-CS conjugate of both P1 and P2 nanoparticles were separately transferred into two different 7 cm-length dialysis membrane (1K) and two tips of membranes were closed with clips. Each nanoparticle-filled membranes were placed in separate beakers and dialyzed against ultra pure water as receptor solutions at 300 rpm. Water inside the beakers was changed with the fresh water for five times. Afterwards, solutions inside the membranes were transferred into eppendorf tubes and stored at +4ºC for further FT-IR measurements.

### 3.2.5. Characterization of FA conjugated Nanoparticles

*Hydrodynamic volume measurement:* Size determination of nanoparticles was done by Dynamic Light Scattering (DLS) measurements in water at 25 °C by Anton Paar Litesizer500 and Wyatt Technologies Dynapro Nanostar. Hydrodynamic diameter and polydispersity index of nanoparticles (AA NP, Cur-AA NP and CS(Cur-AA NP)) were measured in distilled water and at room temperature. 1 mL of these solutions was

transferred into glass cuvette and run for 10 process run with 5 sec equilibrium time for three repetitions.

*Surface charge measurement:* Surface charge evaluation of AA NP, Cur-AA NP and CS(Cur-AA NP) was done by Anton Paar Litesizer500 at 25 °C with 100 runs for three repetitions.

*Morphological analysis:* The morphology of obtained nanoparticles was examined by Transmission electron microscopic (TEM) (Thermo Fischer Scientific, Talos L120C) operated at 20kV with 3.5 spot size and support-cupper TEM grids were utilized to visualize nanoparticles.

*Functional Group Analysis:* Freeze-dried functionalized nanoparticles were investigated for their primary functional moieties in order to check FA-CS conjugation process by Fourier Transform Infrared Spectroscopy (FT-IR) (Thermo Fisher Scientific Inc.; Nicolet 380).

*Determination of Encapsulation Efficiency:* Encapsulation efficiency values were investigated by LC-MSMS instrument (Agilent Technologies 1260 Infinity II). Briefly, standard curve of curcumin was plotted with serial diluted samples with concentrations of 25, 50, 100, 200, 500, 1000, 2500, 5000, 7500, 10000 ppb. The calibration curve was drawn against mass peak intensity of molecular ion with m/z ratio as 365.2. In order to measure the amount of drug molecules loaded in the nanoparticles, dialysis-purified drug-loaded nanoparticles were incubated in DMF/water mixture with the ratio of 1:1:4 (NP:DMF:DW) for their dissociation and liberation of the drug molecules into the solution. Released curcumin amount was examined with the prepared calibration curve and amount of curcumin at each sample was calculated via equation of this curve.

For the drug-loaded nanoparticles, encapsulation efficiency values were determined based on the following equation 1 (eq.1):

*Encapsulation Efficiency:* $(m_{\text{loaded drug}} / m_{\text{Initial drug}})*100$ (eq.1)

#### 3.2.5.1. Stability Study for Nanoparticles

Stability of nanoparticles was studied via size measurement by DLS depending on hydrodynamic diameter change day by day. Briefly, nanoparticle solution was transferred into glass cuvette and run for 10 process run with 5 sec equilibrium time for three times Hydrodynamic diameter of nanoparticles (AA NP, (Cur-AA NP), CS(Cur-AA NP) and FA-CS(Cur-AA NP)) for both of them obtained by following Procedure 1 (P1) and Procedure 2 (P2) were measured successively. Size measurements were taken at different time intervals from day 0 to day 10.

### 3.2.6. Drug Release Profiles of Functionalized Nanoparticles

Determination of release profiles of drug molecules from the drug-loaded nanoparticles was studied in both 10 mM Phosphate Buffered Saline (PBS) (pH 7.4) and Sodium Acetate Buffer (SAB) (pH 5.5) in order to mimic human body fluids as healthy and inflammated conditions, respectively. Briefly, drug release setup was prepared as follows; 1 mL of CS(Cur-AA NP) and FA-CS(Cur-AA NP)) (both P1 and P2, separately) was transferred into a 7 cm-length dialysis membrane (1K) and two tips of membrane were closed with clips. Each nanoparticle-filled membrane was put into separate falcon tubes that were filled with either 30 mL PBS or 30 mL SAB. Falcon tubes were incubated in thermal-shaker at 37 ºC to mimic human body temperature and thermal-shaker was rotated at 200 rpm during the experiments. First sample at time 0 ($t_0$) was taken initially and then samples from the receptor buffer solutions were collected at different time intervals for 0.25, 0.5, 1, 2, 4, 6, 8, 12, 24, 48, 72 and 96h. Samples were stored at -20 ºC for LC-MS/MS measurements.

### 3.2.7. Preparation of Nanoparticle-Embedded Hydrogel Scaffolds (HG/CS(AA_NPs))

PNIPAM based hydrogel scaffolds were prepared by following literature procedures with slight modifications (34). Hydrogels without nanoparticle (blank) was also prepared for its comparison with the drug-loaded nanoparticle embedded hydrogel structure.

Briefly, blank hydrogel was prepared as follows; 100 mg of powder PNIPAM (~40000 MW) was dissolved in 900 µL ultra pure water in an eppendorf tube. This solution was sonicated to get rid of the lumps and bubbles, and then stored at +4 ºC. On the other side, the cross-linker for the hydrogel synthesis, namely (tetraethylene glycol dimethacrylate) was filtered through Aluminum oxide to remove inhibitor inside it. 20.5 µL of this cross-linker was added onto the PNIPAM solution and vortexed gently. Lastly, 50 µL of 5% APS (in $H_2O$ by w/v) and 30 µL TEMED were added in this solution as initiator and accelerator, respectively. By this step, crosslinking and entrapment of PNIPAM polymer chains in ethylene glycol network was initiated. The reaction mixture placed eppendorf tube was shook by vortex shortly and then placed into thermal-shaker. The mixture was placed in thermal-shaker for complete gel formation at 37.5 ºC for overnight.

Nanoparticle (with or without drug) embedded hydrogels were prepared as follows; 100 mg of powder PNIPAM (~2000 MW) was dissolved in 700 µL ultra pure water in an eppendorf tube. Then the solution was sonicated to get rid of the lumps and bubbles, and stored at +4 ºC until the addition of 20.5 µL of Al2O3 filtered tetraethylene glycol dimethacrylate as cross-linker and vortexed gently. 200 µL from nanoparticle solutions

(prepared by either P1 or P5; CS(Cur-AA NP) and FA-CS(Cur-AA NP))) was added and shook upside down softly. Initiator complex, 50 μL APS (5% w/v) and 30 μL TEMED, was added in the polymer-crosslinker mixture. Eppendorf tube was shook by vortex shortly and then placed into thermal shaker at 37ºC for overnight for complete gel formation.

### 3.2.8. Characterization of Nanoparticle-Embedded Hydrogel Scaffolds

Degradation studies, swelling behavior, thermo-responsive (injectability) property and morphology of nanoparticle-embedded hydrogel scaffolds were investigated in the context of this thesis. The scanning electron micrography (SEM) images were obtained using Thermo Fischer Scientific Quanta 650 FEG. SEM samples were prepared by coating gold and not dried with carbon tape on stub. Rheological properties were conducted on a Malvern Kinexus rheometer.

#### 3.2.8.1. Rheological Test of Nanoparticle-Embedded Hydrogel Scaffolds

Gelation process and degradation properties of hydrogel were measured with J2 SR 4703 SS geometry. Degradation property was studied by taking measurements at parameters between $\gamma = 0.001$ and $\gamma = 1$ at $f = 1$ Hz at 37 ºC. The gelation process was analyzed under CD-auto strain mode with $\gamma = 0.01$ at $f = 1$ Hz. The strain-dependent oscillatory rheology and frequency dependent oscillatory rheology of hydrogel scaffolds were tested at 0.1 Hz, 50.5 Hz, 100 Hz and $\gamma = 0.01$ at 37 °C.

#### 3.2.8.2. Thermo-responsiveness of Nanoparticle-Embedded Hydrogel Scaffolds

Thermo-responsive property of hydrogels was investigated with a set up that includes a piece of freshly obtained chicken breast tissue (4 cm x 4 cm). Briefly, a small scratch

(1 cm) was scared on tissue surface to mimic a wound. Tissue sample was placed in the thermal shaker and temperature of specifically tissue sample was adjusted to 37 ºC and checked by a digital thermometer. Liquid mixture was prepared as reported before (3.3). Then this mixture was immediately injected into scratch site with syringe and allowed to spread inside the scratch. As it is, tissue sample was stored in thermal shaker at 37 ºC for further observation of gelation process and wound closure.

#### 3.2.8.3. Swelling Capacity of Nanoparticle-Embedded Hydrogel Scaffolds

Swelling behaviors of the hydrogels (with and without nanoparticle) were investigated by calculating water uptake percentage as a function of time until an equilibrium condition is observed. Briefly, swollen a piece of hydrogel was frozen at -20 ºC and then freeze-dried in lyophilizer. Dry hydrogel sample was transferred into a beaker containing deionized water. Increase in the weight of hydrogel was recorded as a function of time for a 30 sec (t0-t15), 2 min (t16-t22), 3 min (t23-t28), 5 min (t29-t30) and 10 min (t30-t31) time points. Obtained data were used to plot the swelling capacity graphs. The swelling ratio percent W was calculated via equation 2 (eq.2) where $m_w$ and $m_d$ are the weights of wet and dry samples, respectively.

$$\% W = (m_w - m_d) / m_d \times 100 \qquad \text{(eq.2)}$$

### 3.2.9. Drug Release Studies of Nanoparticle-Embedded Hydrogel Scaffolds

Phosphate buffered saline (PBS) (pH 7.4) and sodium acetate buffer (SAB) (pH 5.5) were used to mimic human body fluids. Briefly, drug release set-up was prepared as follows; nanoparticle embedded gels ((FA-CS(Cur-AA NP) formed with both P1 and P2, separately) was transferred into 7 cm-length dialysis membrane (1K) and two tips of membrane were closed with clips. Gel-containing membranes were put into falcon

tubes that filled with 30 mL PBS or 30 mL SAB, separately. Falcon tubes were placed in beaker to stand and beakers were placed in thermal-shaker. Temperature was adjusted to 37 ºC to mimic human body temperature and thermal-shaker was rotated at 200 rpm. Samples were collected at each half an hour, up to 12h and then 24h, 48h, 72h and 96h samples were taken afterwards. All collected samples were stored at -20 ºC for LC-MS/MS measurements.

# 4. RESULTS

## 4.1. Preparation of Drug Delivery System

### 4.1.1. Preparation of Alginate Nanoparticles (AA-NPs)

Measurements (intensity)

| Name | Temperature [°C] | Processed runs | Measurement position [mm] | Polydispersity index [%] | Hydrodynamic diameter [nm] | Peak 1 (intensity) [nm] | Peak 2 (intensity) [nm] | Peak 3 (intensity) [nm] | Diffusion Coefficient [µm²/s] | Color |
|---|---|---|---|---|---|---|---|---|---|---|
| BSA | 25,0 | 10 | 0,0 | 25,1 | 6,81 | 2,84 | 22,79 | 414,0 | 72,0 | |
| 50 AinC | 25,0 | 10 | 0,4 | 57,5 | 9942 | 274,9 | 2640 | - | 0,0 | |
| 50 AinC F | 25,0 | 10 | 0,0 | 359,1 | 3,35 | - | - | - | 146,3 | |
| 50 AinC L | 25,0 | 10 | 0,0 | 36,3 | 21801 | 391,6 | - | - | 0,0 | |
| 50 AinC L F | 25,0 | 10 | 0,0 | 376,2 | 24,43 | 91,12 | 4,59 | - | 20,1 | |
| 75 AinC | 25,0 | 10 | 0,0 | 562,1 | 2626 | 1107,7 | 3778 | - | 0,2 | |
| 75 AinC F | 25,0 | 10 | 0,9 | 54,7 | 1043,0 | 243,6 | 0,52 | - | 0,5 | |
| 75 AinC L | 25,0 | 10 | 0,6 | 47,2 | 3748 | 139,71 | 3002 | 12,46 | 0,1 | |
| 75 AinC L F | 25,0 | 10 | 0,0 | 45,6 | 3219 | 211,8 | 2984 | 39,57 | 0,2 | |

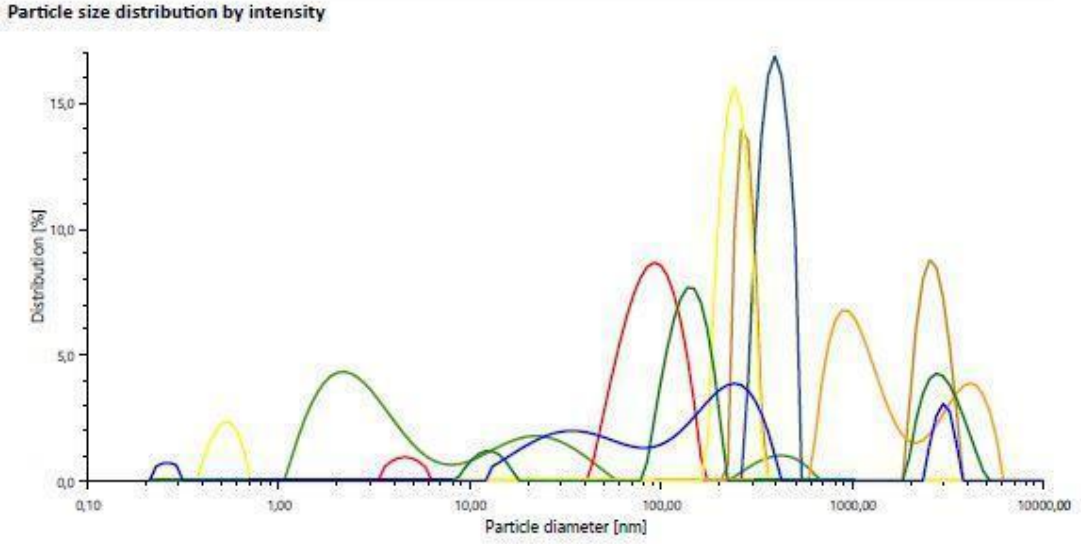


**Figure 10.** Comparison of prepared alginate nanoparticles with different calcium chloride concentrations

Measurements (intensity)

| Name | Temperature [°C] | Processed runs | Measurement position [mm] | Polydispersity index [%] | Hydrodynamic diameter [nm] | Peak 1 (intensity) [nm] | Peak 2 (intensity) [nm] | Peak 3 (intensity) [nm] | Diffusion Coefficient [µm²/s] | Color |
|---|---|---|---|---|---|---|---|---|---|---|
| 1L F SDS 2ml 25T | 25,0 | 10 | -0,2 | 17,8 | 238,5 | 247,9 | - | - | 2,1 | |
| 3L F SDS 2ml 40T | 25,0 | 10 | -0,3 | 25,4 | 227,0 | 237,2 | 4113 | - | 2,2 | |
| 2L F SDS 3ml 25T | 25,0 | 10 | -0,2 | 15,5 | 183,09 | 178,75 | - | - | 2,7 | |
| 4L F SDS 3ml 40T | 25,0 | 10 | -0,3 | 23,2 | 122,15 | 135,36 | 11970 | - | 4,0 | |

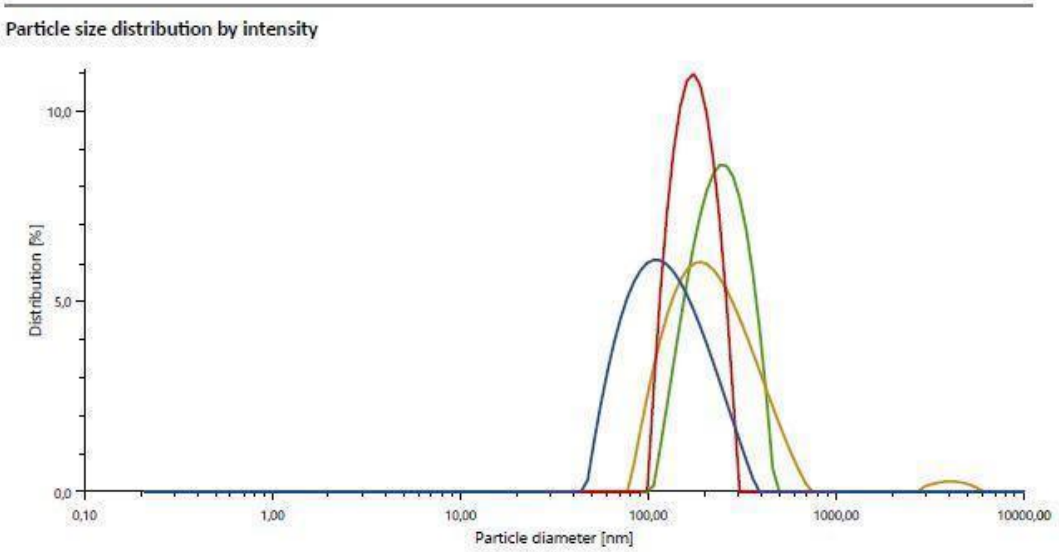


**Figure 11.** Effect of different amount of surfactant and different temperature on preparation of alginate nanoparticles

**Table 1.** Effect of different amount of surfactant and different temperature on preparation of alginate nanoparticles in Procedure 1

| No | $CaCl_2$ (50 mM) (mL) | NaAlg (0.5%) (mL) | L-Lysine (0.1%) (mL) | SDS (0.1%) (mL) | Temp (°C) |
|---|---|---|---|---|---|
| **1** | 4.75 | 0.25 | 2 | 2 | 25 |
| **2** | 4.75 | 0.25 | 2 | 2 | 40 |
| **3** | 4.75 | 0.25 | 3 | 3 | 25 |
| 4 | 4.75 | 0.25 | 3 | 3 | 40 |

**Table 2.** Effect of different amounts of surfactant and different temperature on preparation of alginate nanoparticles in Procedure 2

| No | $CaCl_2$ (0.1%) (mL) | NaAlg (0.1%) (mL) | Tween 80 (2%) (mL) | Tween 80 (1%) (mL) | Temp (°C) |
|---|---|---|---|---|---|
| **1** | 5 | 5 | 6 | - | 25 |
| **2** | 5 | 5 | 6 | - | 40 |
| **3** | 5 | 5 | - | 6 | 25 |
| 4 | 5 | 5 | - | 6 | 40 |

### 4.1.2. Preparation of Curcumin-loaded Chitosan-coated Alginate Nanoparticles (CS(AA-Cur-NPs))

**Surface Charge Measurement**

Procedure 1

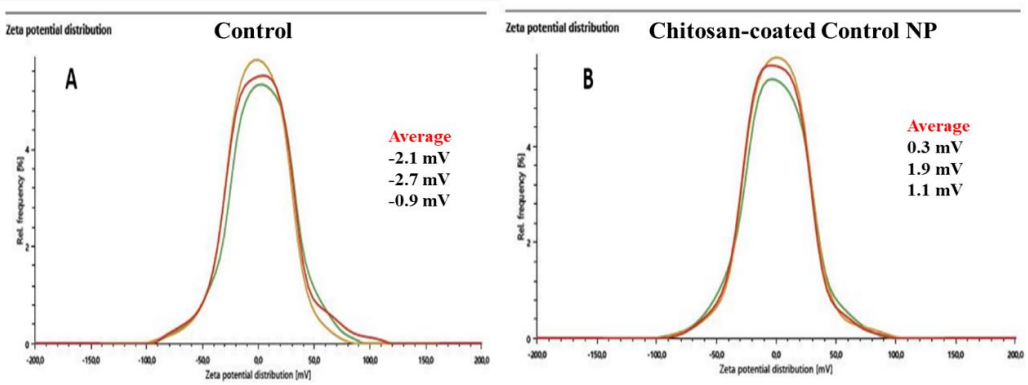


**Figure 12.** Zeta potential graphs of (A) control NP in P1 and (B) chitosan-coated control NP in P1

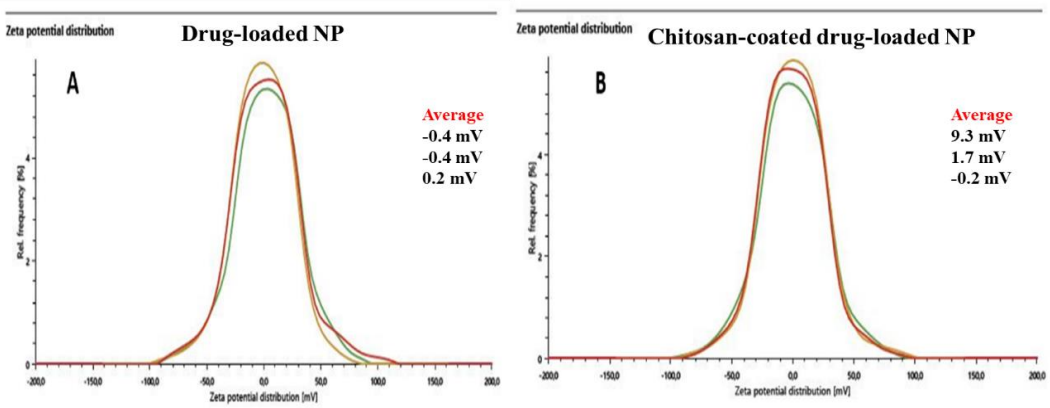


**Figure 13.** Zeta potential graphs of (A) drug-loaded NP in P1 and (B) chitosan-coated drug-loaded NP in P1

Procedure 2

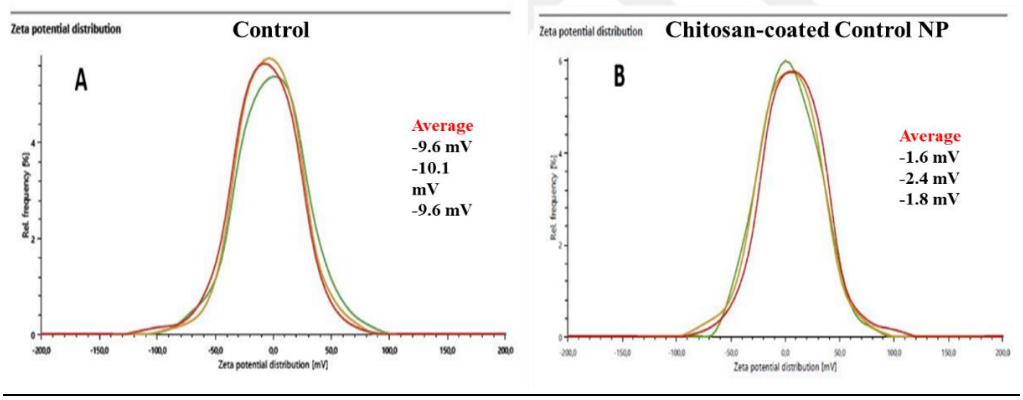


**Figure 14.** Zeta potential graphs of (A) control NP in P2 and (B) chitosan-coated control NP in P2

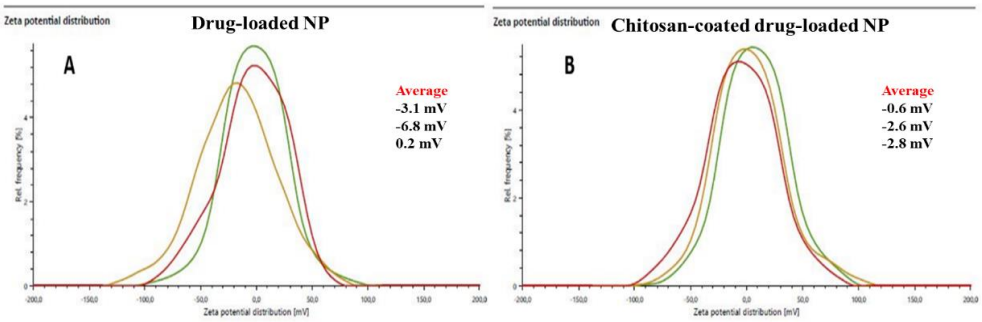


**Figure 15.** Zeta potential graphs of (A) drug-loaded NP in P2 and (B) chitosan-coated drug-loaded NP in P2

### 4.1.3. Functionalization of the Nanoparticle Surface with Folic Acid (FA)

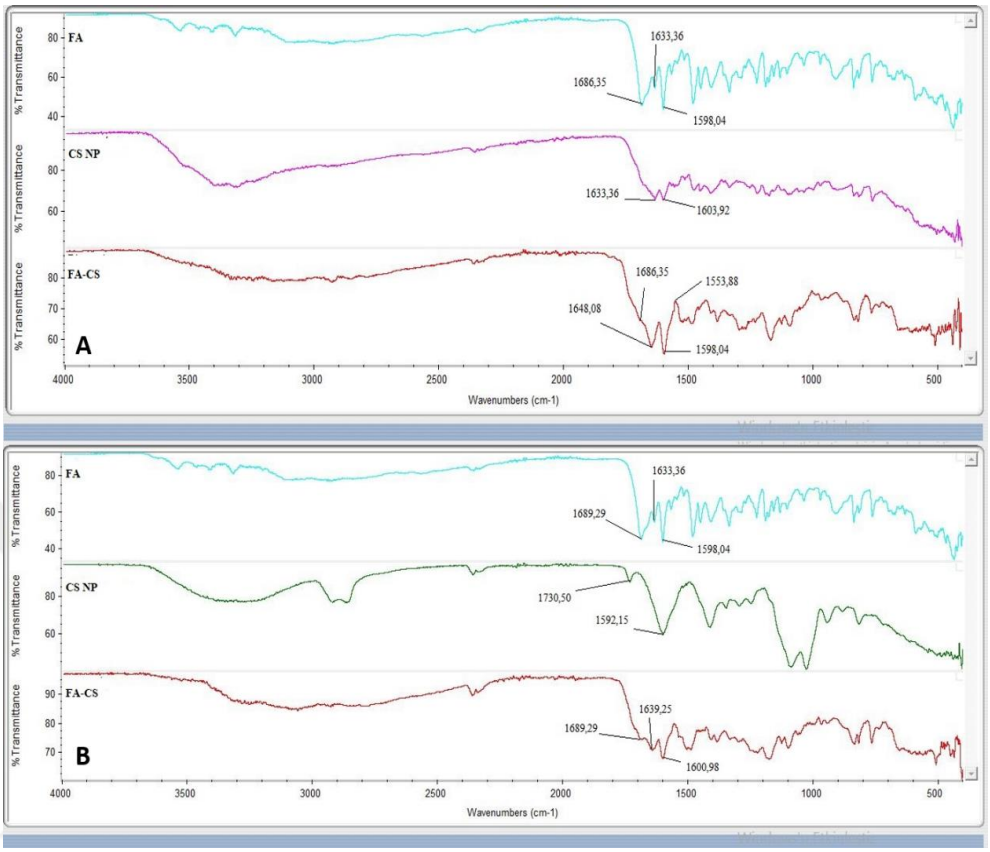


**Figure 16.** FTIR spectra of (A) FA conjugated P1 nanoparticles and (B) FA conjugated P2 nanoparticles

### 4.1.4. Characterization of Functionalized Nanoparticles

**Hydrodynamic volume measurement**

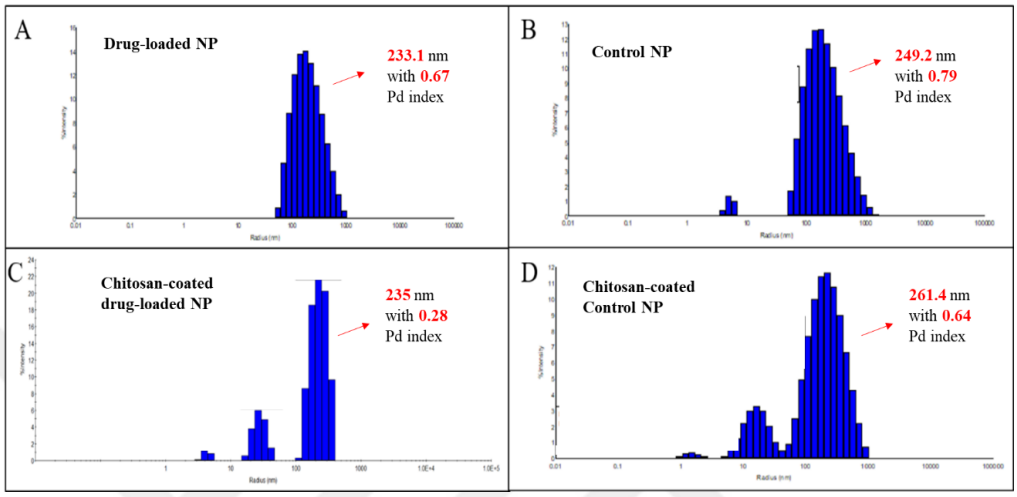


**Figure 17.** Size determination of P1 nanoparticles with Dynamic Light Scattering. (A) Drug-loaded NP in P1 (B) Control NP in P1 (C) Chitosan-coated drug-loaded NP in P1 (D) Chitosan-coated control NP in P1

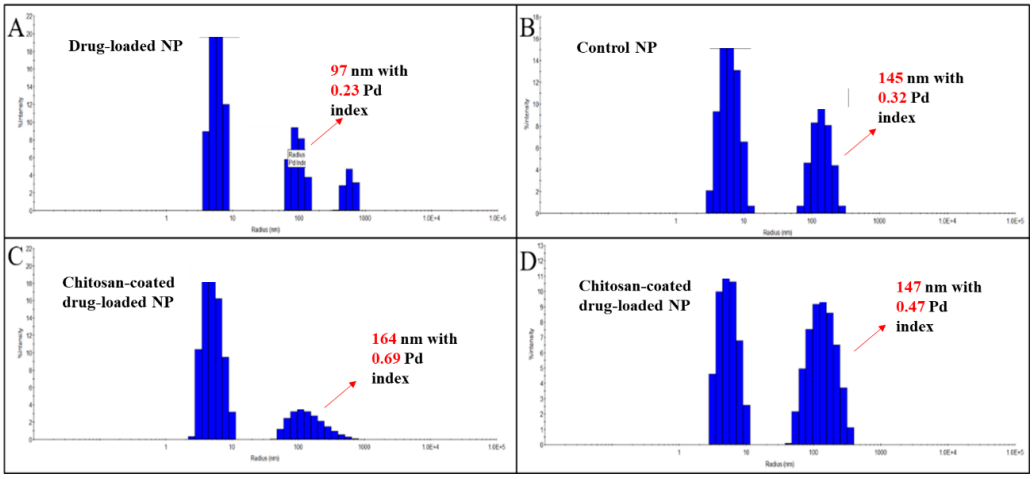


**Figure 18.** Size determination of P2 nanoparticles with Dynamic Light Scattering. (A) Drug-loaded NP in P2 (B) Control NP in P2 (C) Chitosan-coated drug-loaded NP in P2 (D) Chitosan-coated control NP in P2

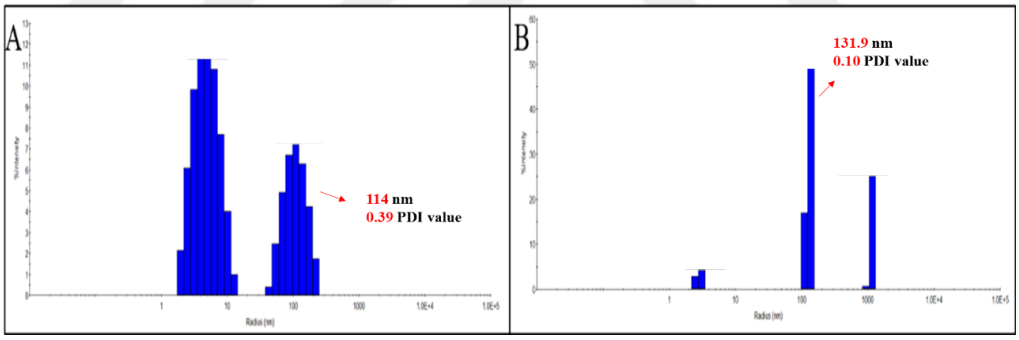


**Figure 19.** Size determination of FA conjugated nanoparticles with Dynamic Light Scattering. (A) FA conjugated NP in P1 (B) FA conjugated NP in P2

## Stability Studies

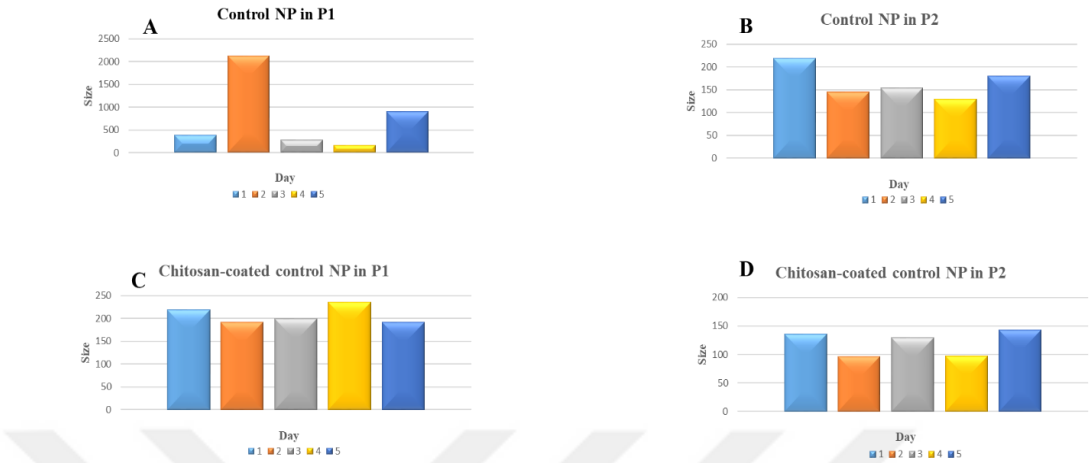


**Figure 20.** Stability Test of (A) Control NP in P1 (B) Control Np in P2 (C) Chitosan-coated control NP in P1 (D) Chitosan-coated control NP in *P2*

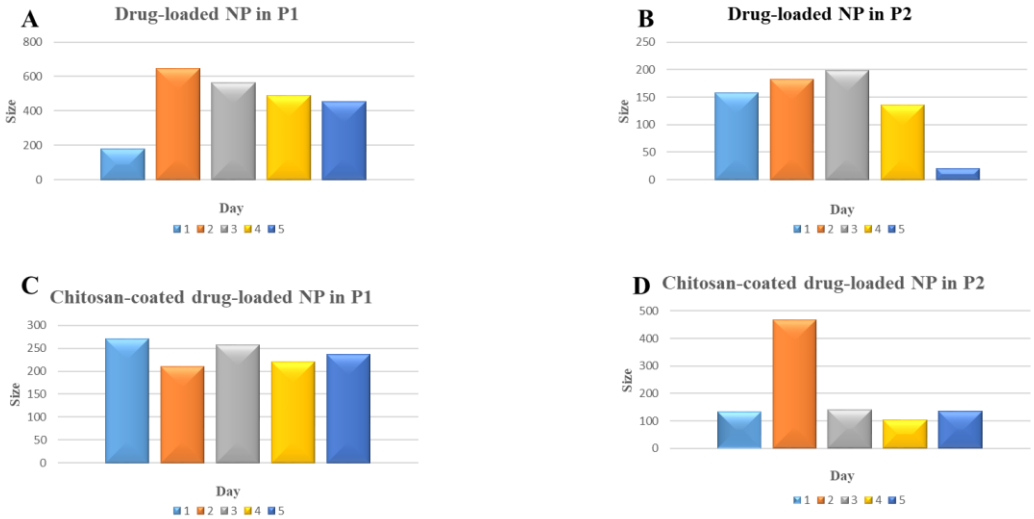


**Figure 21.** Stability Test of (A) Drug-loaded NP in P1 (B) Drug-loaded NP in P2 (C) Chitosan-coated drug-loaded NP in P1 (D) Chitosan-coated drug-loaded NP in P2

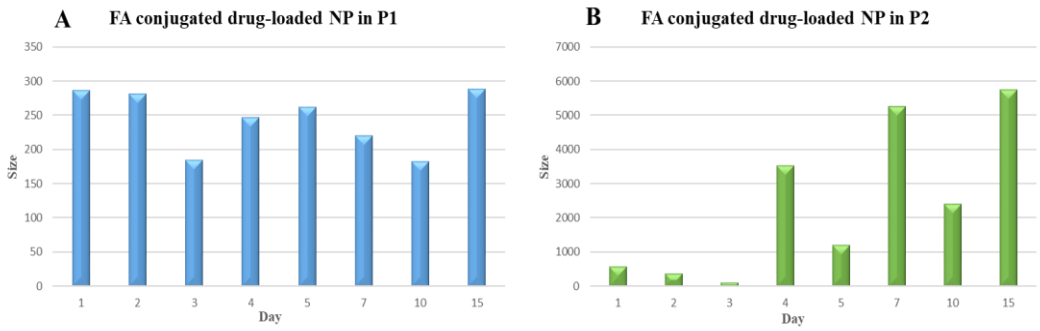


**Figure 22.** Stability Test of (A) FA conjugated NP in P1 (B) FA conjugated NP in P2

**Morphological Analysis via SEM Microscopy**

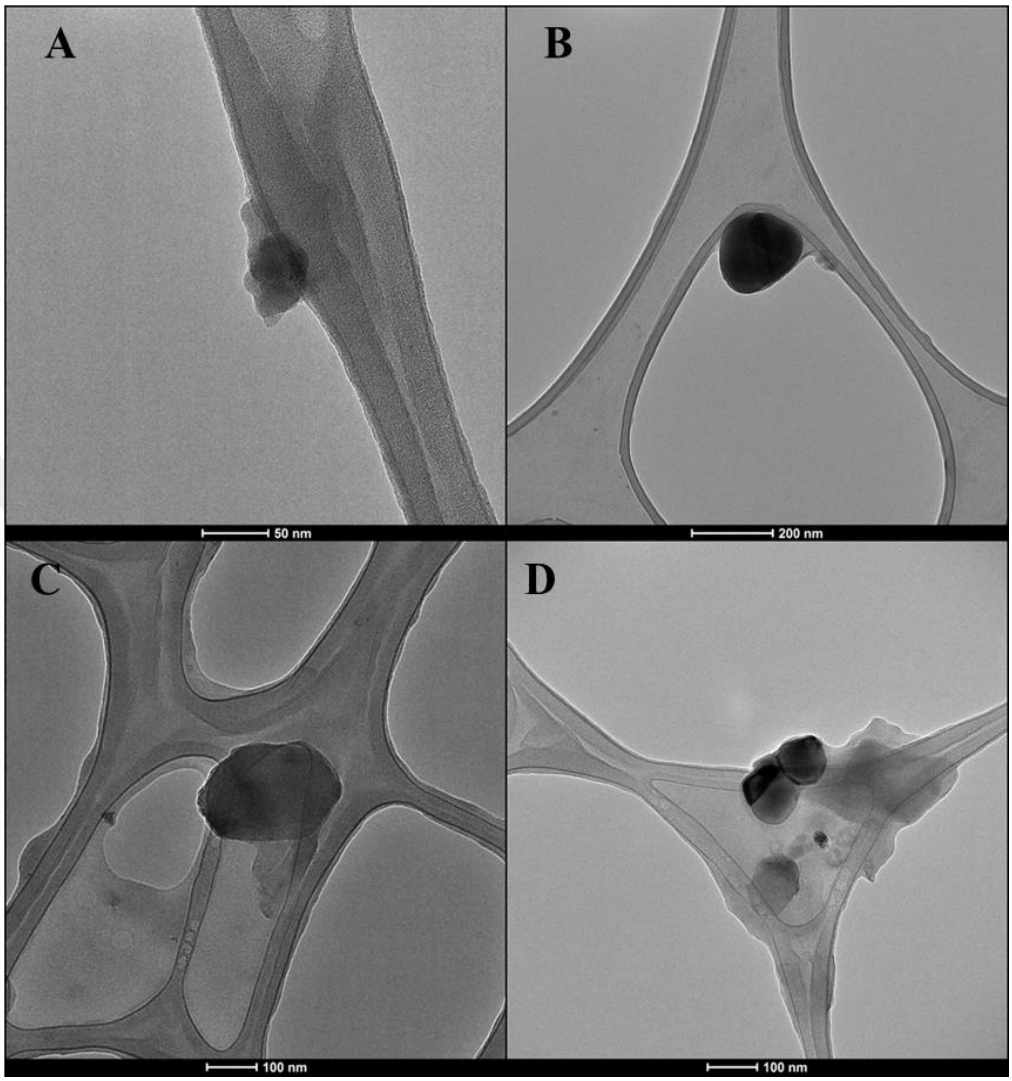


**Figure 23.** Morphological evaluation of P1 nanoparticles with Transmission Electron Microscopy. (A) Control NP in P1 (B) Drug-loaded NP in P1 (C) Chitosan-coated control NP in P1 (D) Chitosan-coated drug-loaded NP in P1

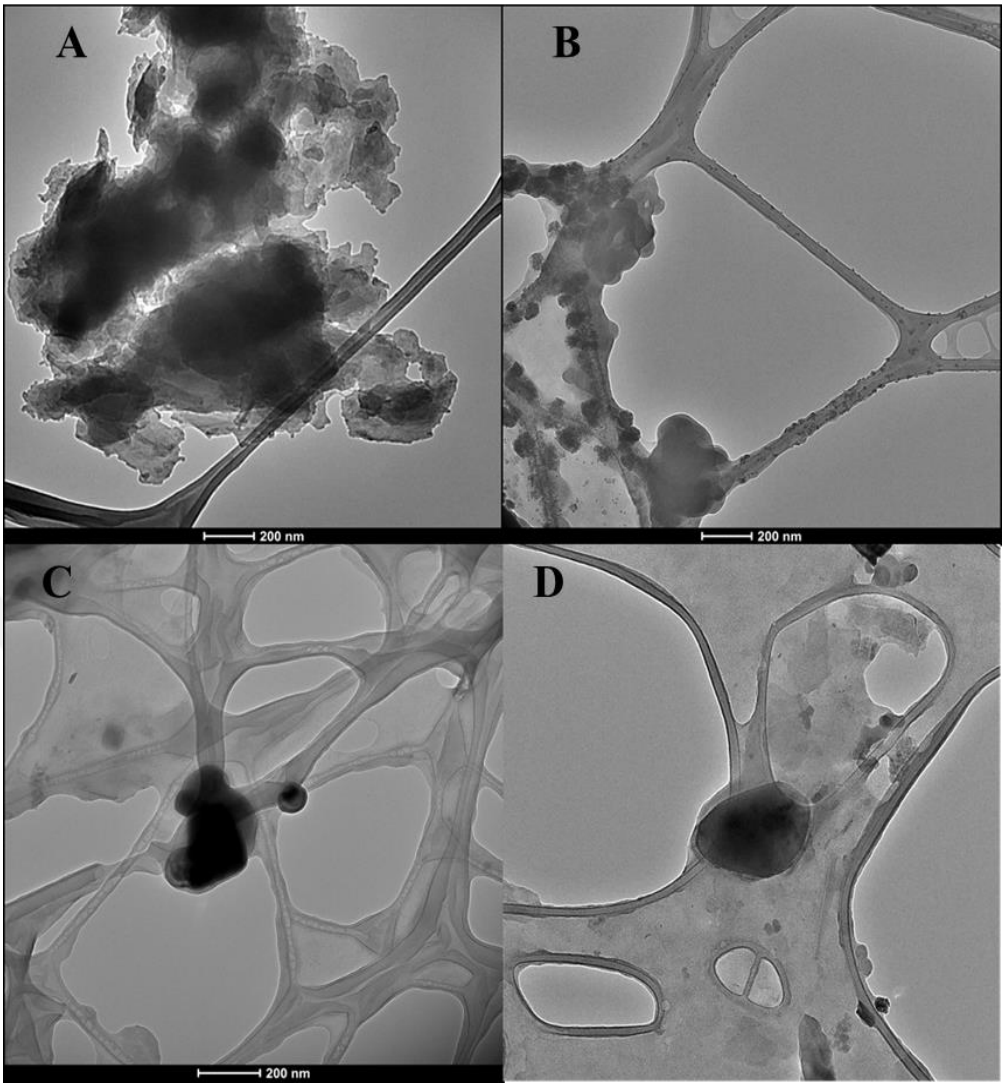


**Figure 24.** Morphological evaluation of P2 nanoparticles with Transmission Electron Microscopy. (A) Control NP in P2 (B) Drug-loaded NP in P2 (C) Chitosan-coated control NP in P2 (D) Chitosan-coated drug-loaded NP in P2

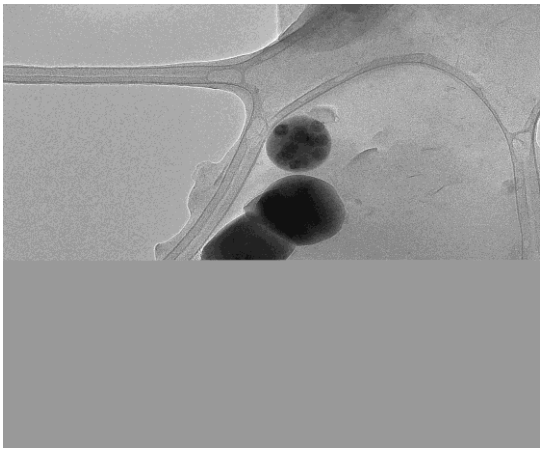

**Figure 25.** Micelle formation in Procedure 2

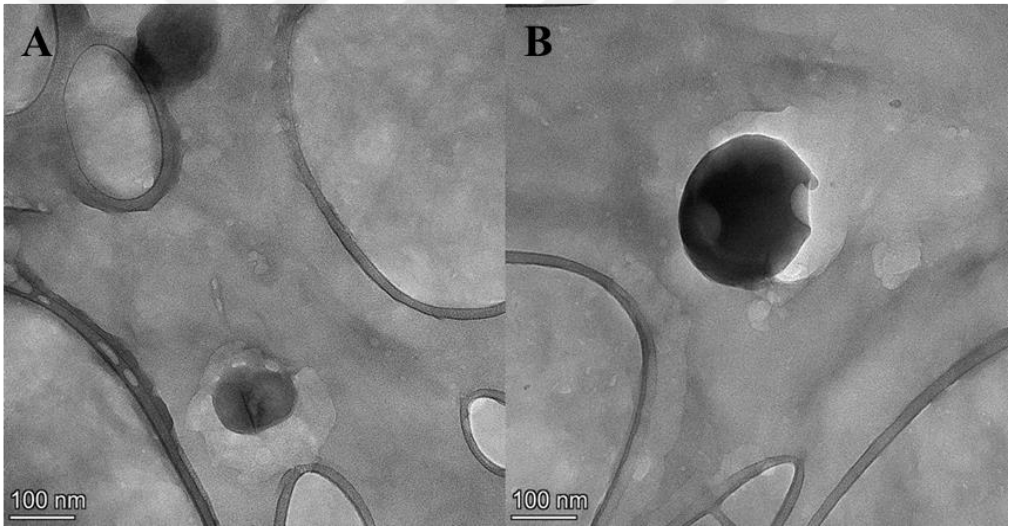


**Figure 26.** Morphological evaluation of FA conjugated nanoparticles with Transmission Electron Microscopy. (A) FA conjugated nanoparticles with in P1 (B) FA conjugated nanoparticles with in P2

## 4.2. Preparation of Nanoparticle-Embedded Hydrogel Scaffolds (HG/CS(AA-Cur_NPs))

### 4.2.1. Characterization of Nanoparticle-Embedded Hydrogel Scaffolds

**Morphological Analysis**

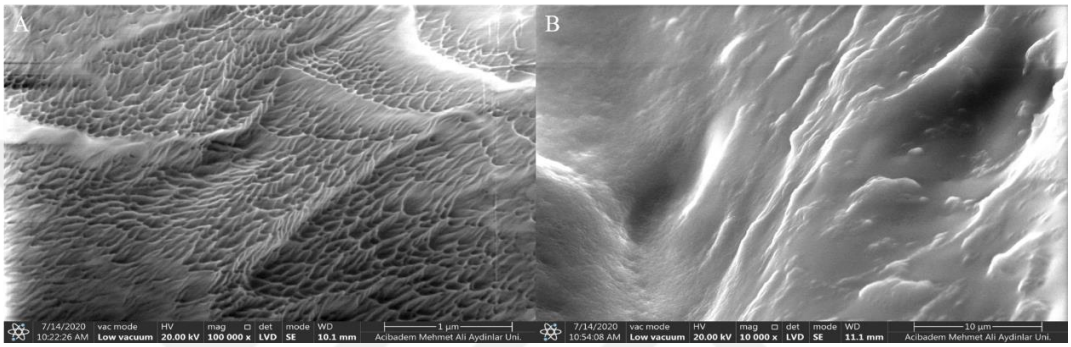


**Figure 27.** Morphological evaluation of control PNIPAM hydrogel scaffolds with Scanning Electron Microscopy. (A) dry (B) wet

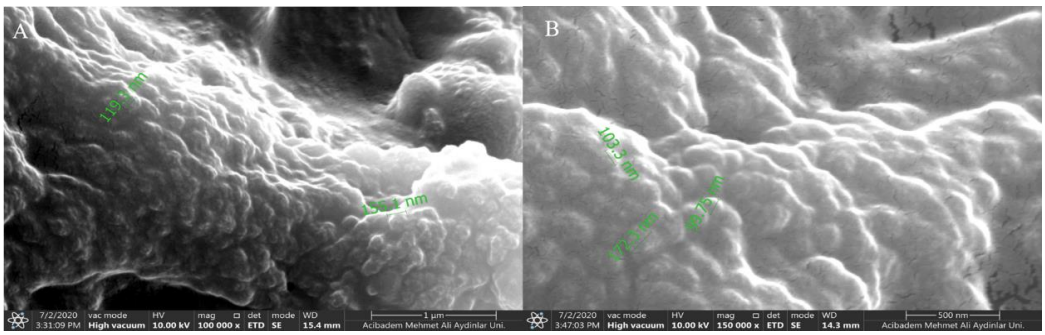


**Figure 28.** Morphological evaluation of pNIPAm hydrogel scaffolds with Scanning Electron Microscopy. (A) P1-NP incorporated pNIPAM hydrogel scaffold (B) P2-NP incorporated pNIPAM hydrogel scaffol

#### 4.2.1.1. Rheological Test of Nanoparticle-Embedded Hydrogel Scaffolds

**Degradation evaluation of thermo-responsive pNIPAM hydrogel scaffolds**

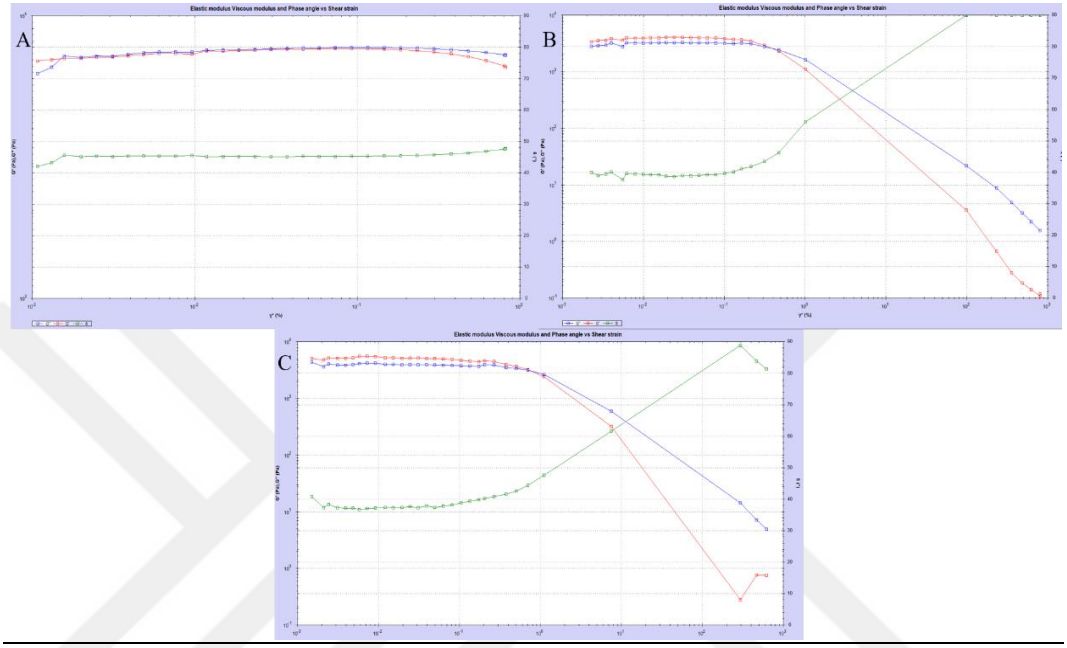


**Figure 29.** Degradation evaluation of pNIPAM hydrogel scaffolds with rheometer. (A) Control pNIPAM hydrogel scaffolds (B) P1-NP incorporated pNIPAM hydrogel scaffolds (C) P2-NP incorporated pNIPAM hydrogel scaffolds

**Gelation evaluation of thermo-responsive pNIPAM hydrogel**

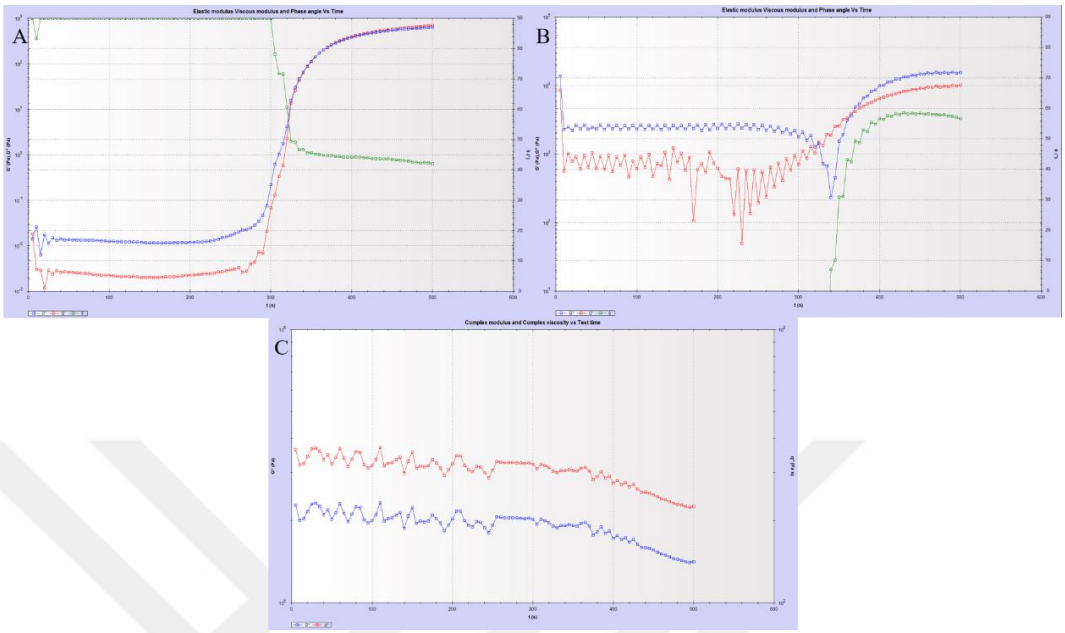


**Figure 30.** Gelation evaluation of control hydrogel scaffolds with rheometer. (A) 0.1 Hz (B) 50.5 Hz (C) 100 Hz

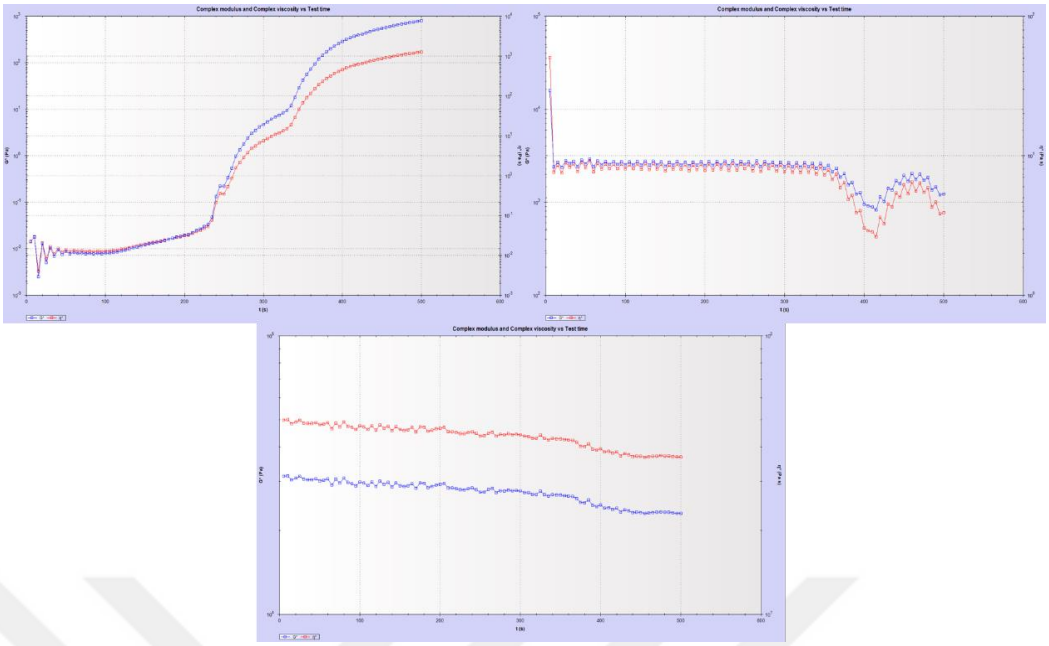

**Figure 31.** Gelation evaluation of P1 nanoparticles incorporated pNIPAM hydrogel scaffolds with rheometer. (A) 0.1 Hz (B) 50.5 Hz (C) 100 Hz

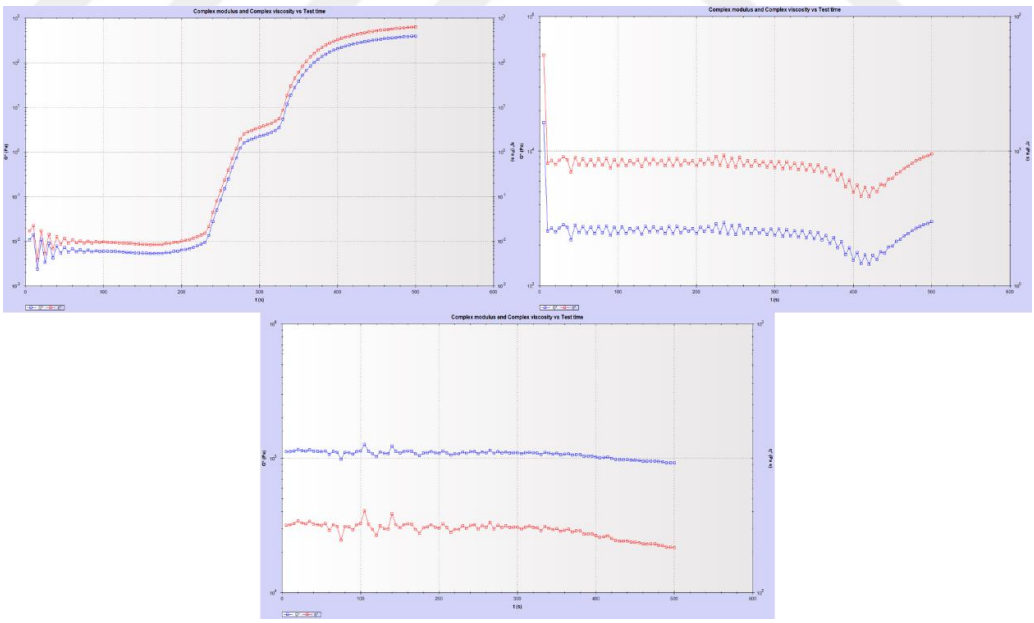

**Figure 32.** Gelation evaluation of P5 nanoparticles incorporated pNIPAM hydrogel scaffolds with rheometer. (A) 0.1 Hz (B) 50.5 Hz (C) 100 Hz

#### 4.2.1.2. Thermo-responsiveness of Nanoparticle-Embedded Hydrogel Scaffolds

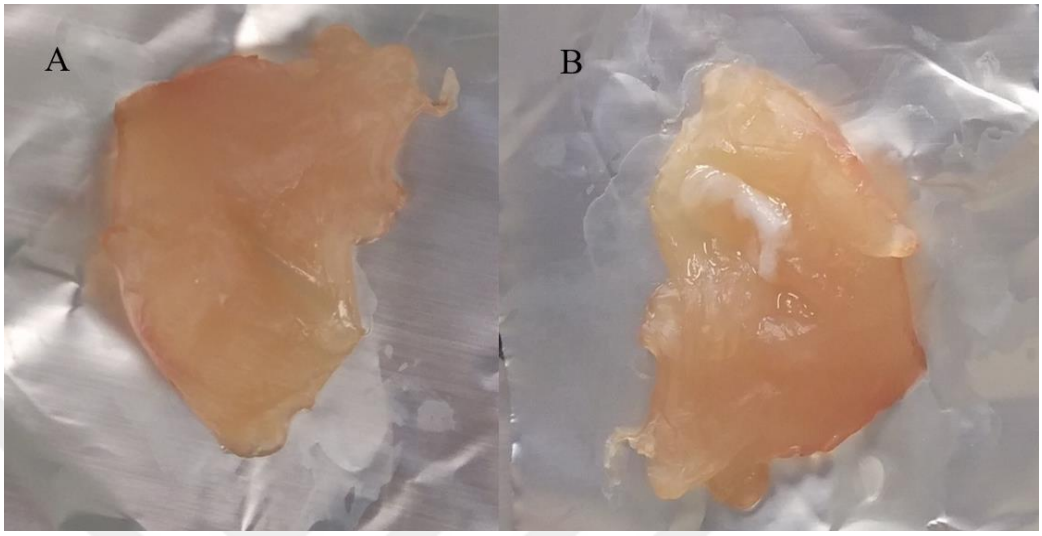


**Figure 33.** Scratch before the injection (A) and after the injection (B) of thermo-responsive pNIPAM polymer mixture

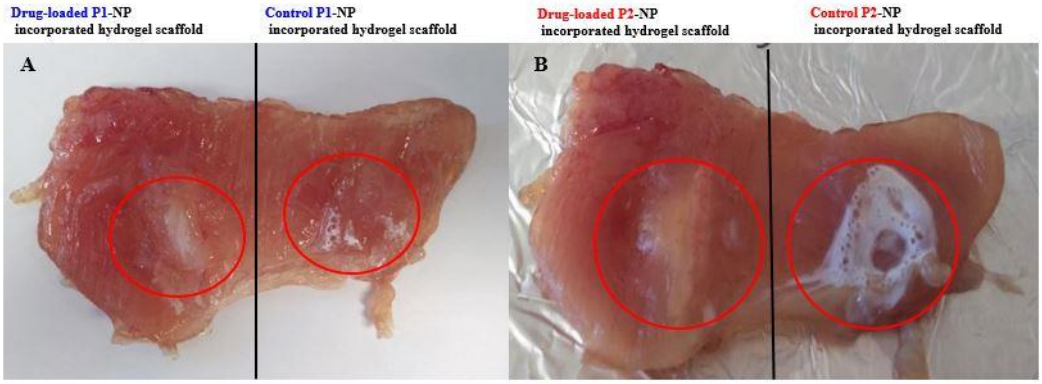


**Figure 34.** After the injection of thermo-responsive pNIPAM hydrogel mixture (A) P1-NP incorporated (B) P2-NP incorporated

**Figure 35.** Degradation of pNIPAM hydrogel scaffold into tissue sample

### 4.2.1.3. Swelling Capacity of Nanoparticle-Embedded Hydrogel Scaffolds

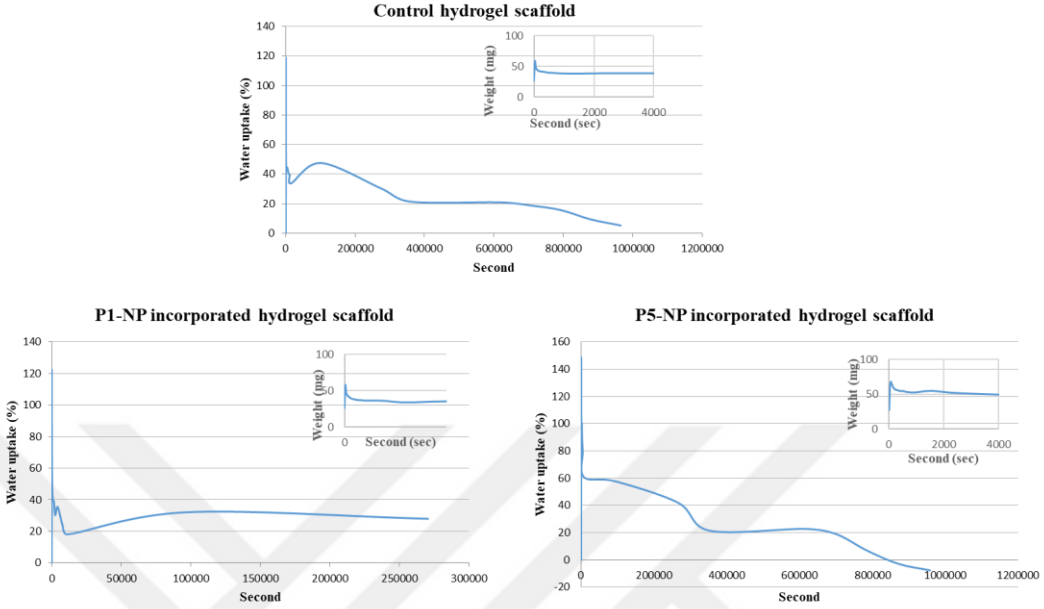


**Figure 36.** Swelling capacity profiles of (A) control hydrogel scaffold (B) P1 nanoparticles incorporated pNIPAM hydrogel scaffold (C) P1 nanoparticles incorporated pNIPAM hydrogel scaffold

## 4.3. Drug Release Profiles of Nanoparticles and Nanoparticle-Embedded Hydrogel Scaffolds

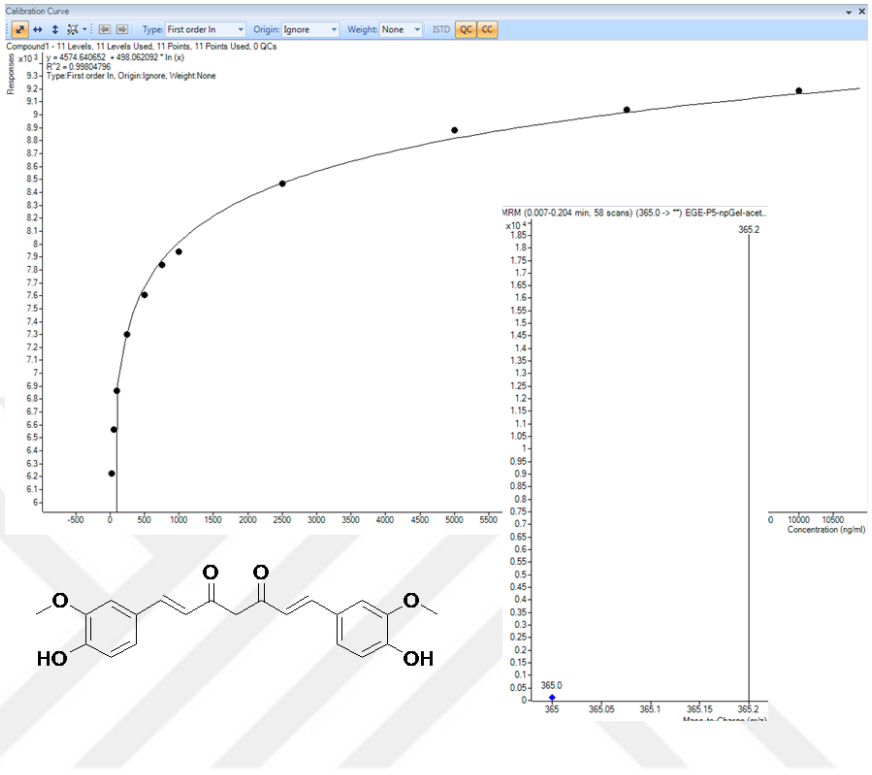


**Figure 37.** Calibration Curve for Curcumin drug molecule drawn by the intensity of mass peak of molecular ion with m/z ratio as 365.2

.

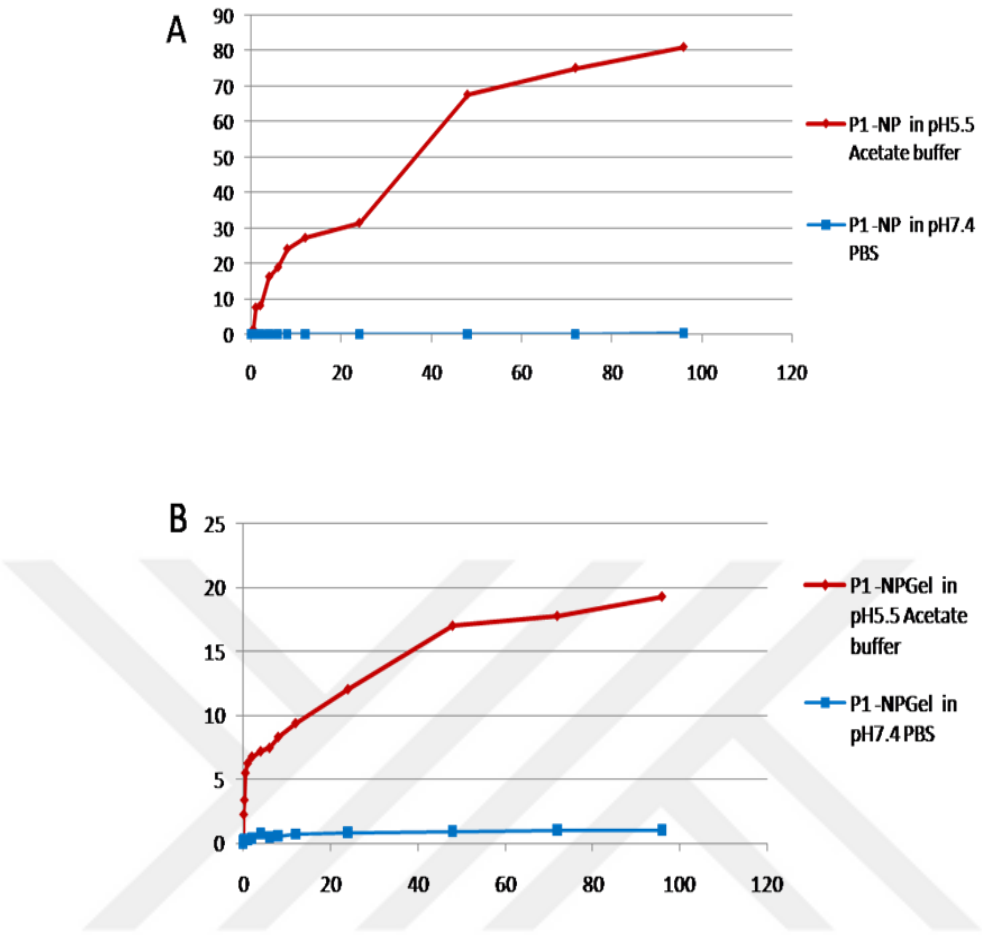


**Figure 38.** Drug release profiles from nanoparticles prepared by Procedure 1 and nanoparticle-embedded hydrogels

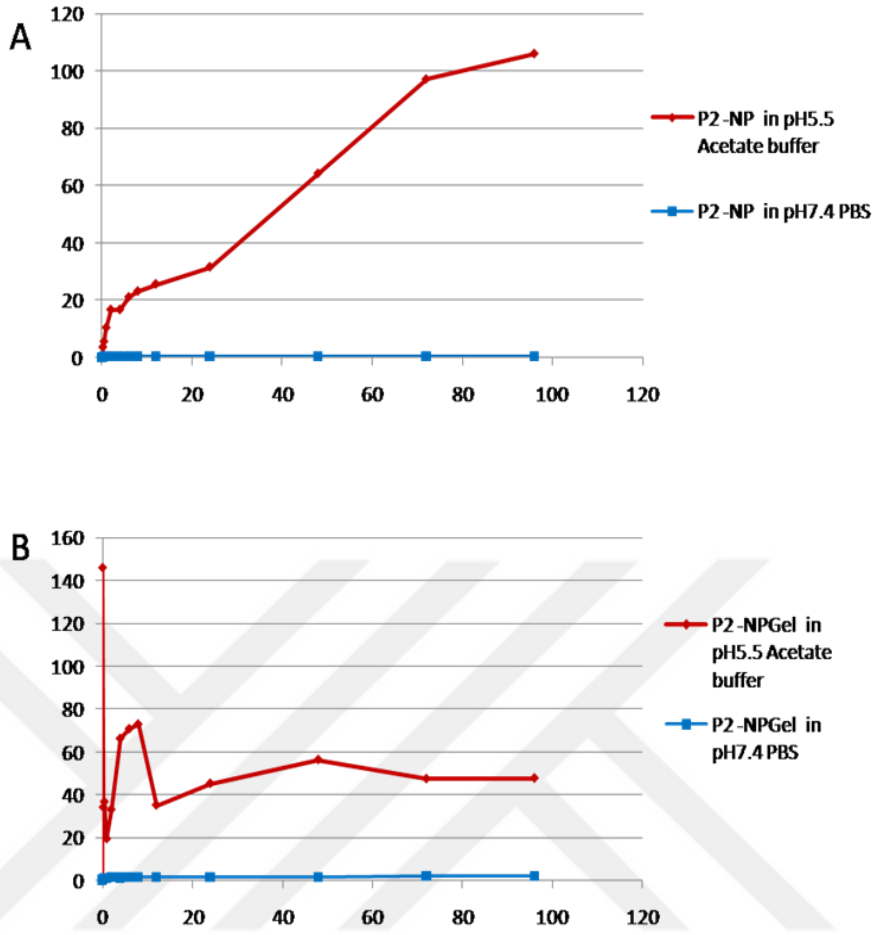


**Figure 39.** Drug release profiles from nanoparticles prepared by Procedure 2 and nanoparticle-embedded hydrogels

# 5. DISCUSSION

Within the scope of the research project, a drug delivery system was prepared that has the potential to allow the therapeutic substances to be administered to a specific part of the body in a minimally invasive way. For this purpose, a biomaterial-based platform has been designed that can release the anti-inflammatory drug active ingredient it contains by injecting it into the damaged tissue after ovarian surgery. Thanks to this system, it is expected that it will be possible to increase the concentration of the relevant active substances locally in the application area and to create a reserve that can release active substance slowly and continuously depending on time.

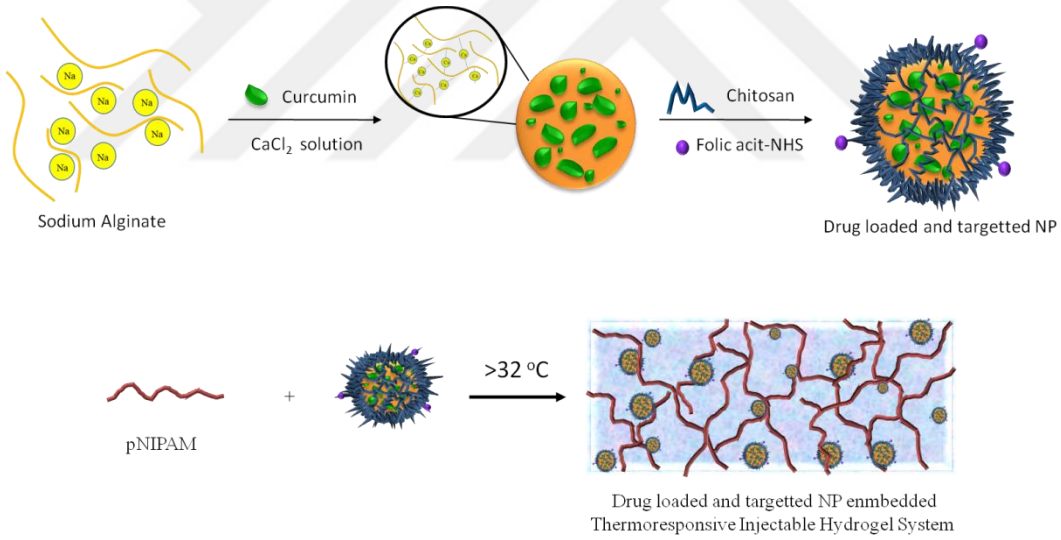


**Figure 40.** Design of the drug-loaded and ovarian cell targeted nanoparticle and its encapsulation into a thermoresponsive and injectable hydrogel scaffold

Two different procedures (P1 and P2) were followed, which depends on two different additives to prepare alginate nanoparticles.

Alginate nanoparticles were prepared through ionic gelation method in Procedure 1, which was explained at Section 2.2.1. Calcium chloride was used as a cross-linker of sodium alginate because reduction reaction occurs that provides alginate and calcium rearrange to form a sphere. Low viscosity sodium alginate was used in order to obtain smaller nanoparticles because the lower gelatinous sodium alginate can bind calcium chloride easier when it compares with high viscosity.

*Figure 10* shows how size distribution is affected by concentration of sodium alginate solution, auxiliary additive and filter process. As seen in *Figure 10*, contrary of procedure in article (37) , sodium alginate solution was added dropwise into calcium chloride solution (AinC). Aggregation was observed in previous experiments while calcium chloride was added into sodium alginate solution. In order to solve this problem and prevent aggregation, it was preferred to add sodium alginate solution into calcium chloride solution dropwise.

50 mM and 75 mM $CaCl_2$ containing nanoparticle solutions were prepared and compared size-wise for better understanding of sodium alginate concentration effect on size distribution for the resultant nanoparticles. Since nanoparticles prepared with low concentration (50mM) of $CaCl_2$ have lower intensity (274.9 nm) as peak 1 when it is compared with nanoparticles prepared with high concentration of $CaCl_2$ (75mM) (1107.7 nm). So, lower concentration of $CaCl_2$ (50 mM) solution was preferred to crosslink sodium alginate for further experimental steps.

As another auxiliary additive that has been used in literature widely, Poly-l-lysine is a polycationic agent that has a net positive charge. Since there is a reduction reaction between alginate and calcium, poly-l-lysine helps matrix formation. In *Figure 11*, letter ‘L’ describes nanoparticles prepared with l-lysine and letter ‘F’ indicates that the

solution has been filtered. 50 AinC, 50 AinC L and 50 AinC L and F nanoparticles were prepared to obtain effect of additives and filtration on size distribution.

Contrary to expectations, 50 AinC L nanoparticles have higher intensity (391.6 nm) with higher polydispersity index (218001) than 50 AinC (274.9 nm) with lower polydispersity index (9942), while filtration (50 AinC L F) helps to obtain lower intensity (91.12 nm) with lower polydispersity (376.2). Reason that observation of higher intensity and higher polydispersity with addition of l-lysine is the imbalance of ionic charge in the experiment solution. To balance ionic charge during the reaction, SDS was used as a negatively charged agent.

When *Figure 10* and *Figure 11* are evaluated together, it can be clearly seen that SDS addition used to balance ionic charge of reaction helps to decrease polydispersity of nanoparticles. Besides the benefits of auxiliary additives on size distribution and polydispersity index, increase in their amounts provides comparably smaller nanoparticles.

Apart from the effects of chemical structures and charges of polymers and additives contributed into the nanoparticle formation, there are several other parameters which may have an impact on the crosslinking and/or self-assembly of polymer chains with each other like temperature and rotation speed. During the optimization procedures for the formation of alginate-based nanoparticles in this thesis, different temperatures and stirring rates were studied and their effect on the size of resultant nanoparticles were determined by size measurements via DLS.

As seen in *Table 1*, two different temperature conditions were investigated additional to increase in the amount of auxiliary additives. In procedure 1 , while 19 to 1 calcium chloride/ alginate ratio was used as in the reference, it is decided to increase surfactant amount as 100%. Procedure was run at room temperature (25C) and 40C and it was shown that higher temperature provides smaller size and better spherical shape.Since it is known that high speed rpm is more effective to obtain smaller nanoparticles, two different rpm values as speed were evaluated.

Filtration, centrifugation and washing steps followed the crosslinking step in order to eliminate aggregates and unbounded molecules and to obtain optimum alginate nanoparticles that have smaller hydrodynamic diameter.

Alginate nanoparticles were prepared through ionotropic gelation method in Procedure 2. Once again; calcium chloride was used as a cross-linker of sodium alginate because of reduction reaction. Low viscosity sodium alginate was used in order to obtain smaller nanoparticles because of the lower gelatin of sodium alginate.

In this procedure, Tween 80 was used as a non-ionic surfactant to provide oily condition during the reaction in order to help formation of more stable nanoparticles. Since tween 80 can form micelle by itself; temperature, rotation speed and concentration of tween 80 bring about by-product during the crosslinking. Since high speed rotation is required for formation of smaller nanoparticles, high speed rotation is desired for the crosslink reaction. But at the same time, high speed rotation increases micelle formation. Therefore, contrary to procedure in the article, lower concentration (1% v/v) of tween 80 was used instead of higher concentration (2% v/v) in order to decrease intensity of micelle in nanoparticle mixture (*Table 2*). As it is expected, the nanoparticles that formed with 1% (v/v) of tween 80 solution has higher intensity than

micelle in the mixture when compared with nanoparticles that formed with 2% (v/v) of tween 80 solution.

Since there are several effects that play a role in preparation of nanoparticles (temperature, spin rate etc.) optimum temperature and rotation speed were investigated. Although high rotation speed brings about micelle formation, but it provides nanoparticles decrement in hydrodynamic diameter and possibility of aggregation.

Although encapsulation of curcumin was done with similar steps in preparation of alginate nanoparticles, there was a quiet obvious effect of loading drug in hydrodynamic diameter. Since curcumin solubility is low in water (0.1 mg/mL) and reaction solutions were prepared with water, the amount of curcumin was investigated. While curcumin was added as a liquid phase because of the solubility in EtOH (10 mg/mL) in Procedure 1, curcumin powder was added in Procedure 2 because of the hydrophobicity that Tween 80 provides. Concentration of curcumin was decided to be 0.1 mg/mL as an optimum condition for both procedures.

Since curcumin is a colorful molecule that has yellowish pigment, color change was observed in the reaction mixture.

Same procedures (for both P1 and P2) were followed to obtain curcumin-loaded chitosan-coated alginate nanoparticles. Chitosan is a positively charged polymer which can surround negatively charged alginate nanoparticles. With the aim of obtaining smaller nanoparticles as far as possible, different MW of chitosan samples

(HMW (310-375 kDa)) and (LMW(5-19 kDa)) with different concentration (1%, 0.5% and 0.1% w/v) and different mixing ratio (1:1, 1:2 and 2:1 (CS:NP)) were investigated. Since HMW (310-375 kDa) chitosan has longer polymer chains and it is heavier, chitosan solution stood as bulk and while chitosan polymer chains are covering alginate nanoparticles they formed thicker layer upon alginate nanoparticles (38). HMW chitosan with higher concentration (1% and 0.5%) solutions were heavier and showed viscos structure because of having more polymer chains, again they formed a thicker layer upon alginate nanoparticles. While alginate nanoparticles were mixing with chitosan solution in order to form chitosan-coated alginate nanoparticles, thinner chitosan layer upon alginate nanoparticles was aimed for keeping the size in the intended size range. In the surface coating step, chitosan had the majority as density in the mixture with 1:1 and 2:1 (CS:NP) ratio. To provide better coating with thinner layer upon alginate nanoparticle, lower chitosan density was chosen Therefore, LMW and lower concentration (0.1% w/v) chitosan solution was used with the 1:2 mixing ratio to enhance chance of coating almost all alginate nanoparticles in the solution.

Since sodium alginate has negative charge and chitosan has positive charge, it was expected that surface coating of alginate nanoparticles would make the surface charge of nanoparticles more positive. Evaluation/elicitation of surface coating via surface charge alteration was done by zeta potential measurement three times repeated at 25 ºC with 100 runs.

Zeta potential measurement of prepared nanoparticles was done with comparison of blank (without drug) and curcumin-loaded (with drug) and chitosan-coated version of these nanoparticle sets. For three times repeated measurements distribution peak (mV) and mean zeta potential (mV) were evaluated. Since mean zeta potential values indicate the state of nanoparticle surface, distribution peak shows charge distribution among the nanoparticles. Besides, zeta potential is important to predict stability of the nanoparticles. It is predicted that if the zeta potential value of a nanoparticle is greater

than +25 mV or less than -25 mV, the nanoparticle has high degrees of stability. However, even though nanoparticles have higher zeta potential value, they get agglomerated and become unstable depending on the preparation materials.

Since alginate is a negatively charged and chitosan is positively charged polymer, it is expected that chitosan-coated nanoparticles should be positively charged in the final state. As seen in *Figure 12*, zeta potential graphs of the nanoparticles prepared with Procedure 1, control (without drug), and chitosan coated version of control nanoparticles. Before the coating the alginate nanoparticles with chitosan (on the left side), although distribution peaks are positive, mean zeta potential of nanoparticles are negative. After coating nanoparticles with chitosan polymer, it is seen that mean zeta potential of nanoparticles are positive. It can be said that alginate nanoparticles were coated with chitosan polymer successfully. Even though the mean zeta potential values are less than +25 mV, stability of nanoparticles should not be evaluated only with zeta potential measurement but also with the help of stability experiments. Stability of nanoparticles will be discussed further.

As seen in *Figure 13*, zeta potential graphs of the nanoparticles prepared with Procedure 1, drug-loaded and chitosan coated version of drug-loaded nanoparticles. Before coating the drug-loaded alginate nanoparticles with chitosan (on the left side), distribution peaks and mean zeta potential of nanoparticles are mostly negative. After coating nanoparticles with chitosan polymer, it is seen that mean zeta potential of nanoparticles are positive. It can be said that alginate nanoparticles were coated with chitosan polymer successfully.

Even though the mean zeta potential values are less than +25 mV, stability of nanoparticles should not be evaluated only with zeta potential measurement but also

with the help of stability experiments. Stability of nanoparticles will be discussed further.

As seen in *Figure 14*, zeta potential graphs of the nanoparticles prepared with Procedure 2, control (without drug), and chitosan coated version of control nanoparticles. Before coating the alginate nanoparticles with chitosan (on the left side), distribution peaks and mean zeta potential of nanoparticles are highly negative. After coating nanoparticles with chitosan polymer, it is seen that mean zeta potential of nanoparticles are still negative but with a lower mV values. Since tween 80 surfactant was used in this procedure and it contributes negative charges, negative value was expected but It can be said that alginate nanoparticles were coated with chitosan polymer successfully.

As seen in *Figure 15*, zeta potential graphs of the nanoparticles prepared with Procedure 2, drug-loaded and chitosan coated version of drug-loaded nanoparticles. Before coating the drug-loaded alginate nanoparticles with chitosan (on the left side), distribution peaks and mean zeta potential of nanoparticles are mostly negative. After coating nanoparticles with chitosan polymer, it is seen that mean zeta potential of nanoparticles are still negative but with a lower mV values. Since tween 80 surfactant was used in this procedure, it contributes negative charges and curcumin is hydrophobic drug which ionization mode is negative, negative value was expected but It can be said that alginate nanoparticles were coated with chitosan polymer successfully.

Functionalization of curcumin-loaded chitosan-coated nanoparticles' surface was made with conjugation reaction of folic acid and chitosan (FA-CS). After dialysis, functionalized nanoparticles were observed by FT-IR spectroscopy *(Figure 16*). It is

clearly seen upon comparison that intensity of the carbonyl peak (1633 $cm^{-1}$) belonging to carboxylic acid group was decreased after conjugation, whereas that of amide group (1686 $cm^{-1}$) has increased simultaneously. Also characteristic peaks of chitosan polymer like –C-O-C- bonds (around 1050 $cm^{-1}$) and O-H &N-H bonds (around 3300 $cm^{-1}$) can be observed at the spectrum of the conjugates obtained by both P1 and P2.

Before conjugating the folic acid onto the surface of chitosan-coated nanoparticles, hydrodynamic volume and polydispersity of nanoparticles were examined.

As seen in *Figure 17*, hydrodynamic volume diagrams of the nanoparticles prepared with Procedure 1, control (without drug), drug-loaded nanoparticles and chitosan coated version of these two nanoparticles. On the right side diagrams, while control nanoparticles were achieved with 249.2 nm size and 0.79 Pd index, coating nanoparticles with chitosan polymer increased the size to 261.4 nm but decreased the Pd index to 0.64. On the left side diagrams, while drug-loaded nanoparticles were achieved with 233.1 nm size and 0.67 Pd index, coating nanoparticles with chitosan polymer increased the size to 235 nm but decreased the Pd index to 0.28. Besides, shorter size distribution columns on the results represent but they were neglected because of the low intensity.

As seen in *Figure 18*, hydrodynamic volume diagrams of the nanoparticles prepared with Procedure 2, control (without drug), drug-loaded nanoparticles and chitosan coated version of these two nanoparticles. On the right side diagrams, while control nanoparticles were achieved with 145 nm size and 0.32 Pd index, while coating nanoparticles with chitosan polymer increased the size to 147 nm, also increasing the Pd index to 0.47. On the left side diagrams, while drug-loaded nanoparticles were achieved with 97 nm size and 0.23 Pd index, while coating nanoparticles with chitosan

polymer increase the size to 164 nm, also increase the Pd index to 0.69. Besides, small size distribution columns (micelle formation) on the results represent  but they were neglected because of the low intensity.

Hydrodynamic volume and polydispersity index of FA conjugated nanoparticles were measured with DLS. As seen *Figure 19*, on the left side, you can see the size distribution diagram of FA conjugated nanoparticles prepared with Procedure 1. FA conjugated nanoparticles were achieved with 114 nm and 0.39 Pd index, but not a majority percentage distribution. On the right side, the size distribution diagram of FA conjugated nanoparticles prepared with Procedure 2 represents. FA conjugated nanoparticles were achieved with 131.9 nm and 0.10 Pd index, with a majority percentage distribution. Smaller size and bigger size distribution columns represent micelle formation and aggregation.

Obtained nanoparticles for both procedures were analysed for their drug encapsulation efficiencies. After nanoparticles were purified from their un-encapsulated drug molecules, their nano and compact sized forms were dispersed with extra PBS/DMF mixture, the samples were analysed at LC-MS MS instrument for the liberated drug molecules that were thought to be free in the solution. By using appropriate calibration curve, amounts of free drug molecules were calculated and compared by the initially loaded drug amounts. As a result, nanoparticles prepared by P1 were shown to encapsulate 99.45% of the loaded drug molecules, whereas P2-NPs were shown to encapsulate only 9.6% of the initial drug loading.

Stability of prepared nanoparticles were evaluated with measurement of size change depending on 5 days. Nanoparticles were stored at + 4° C and sizes were measured with DLS everyday. Here you can see the stability graphs of control (without drug) and chitosan-coated version of control nanoparticles prepared with both P1 and P2

(*Figure 20*). Except control nanoparticles prepared with P1, up to day 5 increment on size of nanoparticle is seen because of the swollen nanoparticles because of the polymers property. Besides, it was expected that chitosan-coated versions of nanoparticles are more stable than the non-coated version. However, there is no significant size change on nanoparticles and it can be said that chitosan-coated control and drug-loaded nanoparticles are stable up to day 5.

Stability graphs of drug-loaded and chitosan-coated versions of drug-loaded nanoparticles prepared with both P1 and P2 (*Figure 21*). For the drug-loaded nanoparticles, there is no slight change in size, except for chitosan-coated versions on day 5. This significant change on chitosan-coated versions caused by swelling, as it is expected. However, it can be said that chitosan-coated control and drug-loaded nanoparticles are stable up to day 5.

Stability of FA conjugated nanoparticles in P1 and P2 were evaluated with measurement of size change depends on 15 days. Nanoparticles were stored at + 4° C and sizes were measured with DLS in certain time intervals. As seen in *Figure 22*, stability graphs of FA conjugated nanoparticles prepared with both P1 and P2. While the nanoparticles prepared with P1 shows no significant size change up to 15 days, nanoparticles prepared with P2 shows significant size change after day 3, because of the swelling and aggregation of micelles.

For the morphological analysis of nanoparticles, transmission electron microscopy was used. TEM images of control(without drug) and drug-loaded alginate nanoparticles and their chitosan-coated versions were captured (*Figure 23*). Sphere shape was observed. On the up-left side, control nanoparticles can be seen in lighter color and drug-loaded version can be distinguished with a dark color on the right side. On the down-left side, chitosan-coated control nanoparticles are represented with a bigger size and again the drug-loaded version can be distinguished with a dark color and with a cloudy chitosan polymer around the nanoparticle.

TEM images of control(without drug) and drug-loaded alginate nanoparticles and their chitosan-coated versions were captured (*Figure 24*). Sphere shape was observed. On the up-left side, control nanoparticles can be seen bulky, this aggregation reason might be repulsive forces because of charges but the drug-loaded version can be distinguished with apparent dark color on the right side. On the down-right side, chitosan-coated control nanoparticles are represent with a bigger size and again the drug-loaded version can be distinguished with a dark color and with a cloudy chitosan polymer around the nanoparticle. Besides, it can be said that the size of nanoparticles match up with DLS results via scale.

However, on the right side image represents the micelle formation in Procedure 2 (*Figure 25*). You can easily see the chitosan covered micelles. Since micelles have a size between 10-15 nm, chitosan polymers gather them and cover.

For the morphological analysis of FA conjugated nanoparticles, transmission electron microscopy was used (*Figure 26*). Spherical shape was observed for both nanoparticles prepared with P1 and P2. Size of nanoparticles match up with DLS result via scale.

Morphological analysis of hydrogel scaffolds was done with SEM to evaluate porous structure. In *Figure 27,* dry and wet control hydrogels were compared to understand the effect of swelling to porous structure. It is seen that wet hydrogel has a smoother structure and apparent porous structure than the dry version. In *Figure 28,* nanoparticle incorporated hydrogel scaffold structures were evaluated with SEM. Incorporated nanoparticles can be seen easily, and size determination can be done even if they are incorporated into hydrogel. On the left side, nanoparticles prepared with P1 and on the right side nanoparticles prepared with P2.

Degradation evaluation of prepared hydrogels were investigated with rheometer. ın *Figure 29*, G'' represents elastic modulus and G' represents viscous modulus. For control, P1-NP and P2-NP incorporated gels, initial states show gel property although P1-NP incorporated gel P2-NP incorporated gel show gel property until cross point where G'' and G' overlap and as G'' and G' diverge P1-NP incorporated gel starts to degradation, as it is expected.

Gelation evaluation of prepared hydrogels were investigated with rheometer according to reference (39), 0.1 Hz, 100 Hz and 50. Hz, average of these frequencies, were examined.

In *Figure 30*, control gel is liquid form at the initial point but after cross point G''diverges, means becoming gel. While P1-NP incorporated gel directly became gel form, P2-NP incorporated gel did not show gelation at 0.1 Hz frequency.

In *Figure 31*, control gel is liquid form at the initial point but after cross point G''diverges, means becoming gel. P1-NP incorporated gel directly became gel because of the high frequency and it protected its viscous modulus property. P2-NP incorporated gel directly became gel and there is no significant degradation at 50.5 Hz frequency.

In *Figure 32*, control and P1-NP incorporated gel directly became gel, but P2-NP incorporated gel protected its elastic property, meaning liquid form. As a result, P1-NP incorporated gel is more stiff but it needs high frequency for gelation and it protects

its gel form longer than P2-NP incorporated gel. P2-NP incorporated gel starts gelation quickly but it degrades at high frequency.

Regarding the construction of hydrogel platform, thermo-responsiveness feature of nanoparticle incorporated hydrogel samples was examined with a simple injection set-up that chicken breast piece was used as tissue sample to substitute or mimic a regular body condition. In *Figure 33*, thermo-responsive property of control hydrogel scaffold was investigated with a set up that includes a piece of freshly obtained chicken breast tissue (4 cm x 4 cm). as it is expected, after injection, the thermo-responsive polymer mixture immediately showed gelation at 37° C and covered the scar.

In *Figure 34*, P1-NP and P2-NP incorporated hydrogels were injected into scar on tissue sample and gelation was observed for both hydrogels, as it is expected.

After injection, tissue sample was stored in thermal shaker at 37 ºC for further observation of the wound closure. In *Figure 35*, degradation of control hydrogel scaffold (without NP) was investigated for 24h. after 24h, it was observed that hydrogel started to degradation.

Swelling test was run for control(without nanoparticle) and nanoparticle prepared with P1 and P2 incorporated hydrogel scaffold.

After lyophilization, dry hydrogels were weighted and put into distilled water to let them swell. At certain time intervals, swollen hydrogels were weighted and noted. With the data, swelling capacity vs time graphs were plotted.

In *Figure 36*, graphs represent the weight of hydrogels depend on increased water content. After time zero, at time 1 interval, hydrogels swelled immediately and then they reached their maximum swelling capacity quickly, as it is expected. Then, swelling of hydrogels continued up to 2 days and then started to degrade.

Curcumin release profiles from both nanoparticles and NP-embedded hydrogels were evaluated (*Figure 37*). In *Figure 38*, NP in P1 and P1-NP incorporated hydrogel drug release profiles was examined. In PBS, there is low release according to acetate buffer, as it is expected. This means, curcumin releases in inflammatory area instead of blood stream. As a result, drug-loaded nanoparticles shows controlled and slow release profile. When nanoparticle incorporated hydrogel release is compared with drug-loaded nanoparticle release, it was seen that the speed of release 4 times, as it is expected.

In *Figure 39,* In PBS, there is low release according to acetate buffer, as it is expected. This means, curcumin releases in inflammatory area instead of blood stream. As a result, drug-loaded nanoparticles shows controlled and slow release profile. When nanoparticle incorporated hydrogel release is compared with drug-loaded nanoparticle release,curcumin release profile is better in nanoparticles. ın gel, curcumin release is lower than drug-loaded nanoparticle, as it is expected. Drug-loaded nanoparticle gel release in the acetate buffer line is not smooth, the reason of this might be caused by measurement error.

# 6. CONCLUSION

The drug delivery system designed in this project is aimed to be used in the treatment of inflammation occurring in the area after ovarian surgery. Functionalized nanoparticles were confined in a polymeric and injectable hydrogel with a slow biodegradation rate and heat sensitive, thereby providing slow and continuous release of the active substance at the target site. Within the scope of the project, nanoparticles whose core is cross-linked and containing curcumin anti-inflammatory agent that will provide inflammation treatment will be prepared.

The core of the carrier proposed in this research project was formed by cross-linking alginate ($Na_2$Alg-$CaCl_2$), a natural polymer that is both biocompatible and biodegradable. In addition to the cross-linked core structure to be trapped, the coating of this nanocarrier with chitosan natural polymer is helpful for the slow release of the drug. Later, the surface of the nanocarrier coated with chitosan natural polymer was functionalized by conjugating the amine groups in the structure of this polymer with folic acid molecules activated with N-hydroxysuccinimide (NHS). Folic acid molecules were attached covalently to the surface of the nanoparticles, so that by binding these drug-loaded nanoparticles to folate receptors, which they see as targets, their accumulation into the ovarian cells would be facilitated and their uptake into the cell are expected to be increased.

The drug loaded nanoparticles prepared were confined in a thermosensitive polymer (pNIPAM), a carrier with a slow biodegradation rate and non-toxic properties. Hydrogels, with their porous structure and high water holding capacity, are limited to three-dimensional cell culture, tissue engineering and drug release, but are used in a wide variety of applications in medical and life science research. pNIPAM polymer, while it is a solution containing polymer in liquid form at room temperature, it

solidifies reversibly with heat and provides a porous hydrogel structure. These pNIPAM chains were crosslinked with a PEG based crosslinker to help the gelation process at body temperature. This polymeric scaffold design was demonstrated to form the hydrogel structure mixed with nanoparticles to gel in a very short time when injected into the tissue wound region at body temperature.

## 7. REFERENCES


**1.** Qiu, Y., & Park, K. (2001). Environment-sensitive hydrogels for drug delivery. Advanced Drug Delivery Reviews, 53(3), 321-339. doi:10.1016/s0169-409x(01)00203-4

**2.** Juliano, R. L. (1978). Drug delivery systems: A brief review. Canadian Journal of Physiology and Pharmacology, 56(5), 683-690. doi:10.1139/y78-112

**3.** N. Bhattarai, J. Gunn, and M. Zhang, "Chitosan-based hydrogels for controlled, localized drug delivery," Adv. Drug Deliv. Rev., vol. 62, no. 1, pp. 83–99, 2010.

**4.** S. Pundir, A. Badola, and D. Sharma, "Sustained release matrix technology and recent advance in matrix drug delivery dystem: A review," Int. J. Drug Res. Tech. Int. J. Drug Res. Technol., vol. 3, no. 1, pp. 12–20, 2013.

**5.** B. Stella et al., "Design of folic acid-conjugated nanoparticles for drug targeting," J. Pharm. Sci., vol. 89, no. 11, pp. 1452–1464, 2000.

**6.** Machado, A. H., Lundberg, D., Ribeiro, A. J., Veiga, F. J., Lindman, B., Miguel, M. G., & Olsson, U. (2012). Preparation of calcium alginate nanoparticles using water-in-oil (W/O) nanoemulsions. Langmuir, 28(9), 4131-4141. doi:10.1021/la204944j

**7.** B. O. Yu, H. C. Tai, W. Xue, L. J. Lee, and R. J. Lee, "Receptor-targeted nanocarriers for therapeutic delivery to cancer," vol. 27, no. October, pp. 286–298, 2010.

**8.** A. Kumari, S. K. Yadav, and S. C. Yadav, "Biodegradable polymeric nanoparticles based drug delivery systems," Colloids Surfaces B Biointerfaces, vol. 75, no. 1, pp. 1–18, 2010.

**9.** R. Singh and J. W. L. Jr, "Nanoparticle-based targeted drug delivery," Exp. Mol. Pathol., vol. 86, no. 3, pp. 215–223, 2009.

**10.** I. R. Scolari, P. L. Páez, M. E. Sánchez-borzone, and G. E. Granero, "Promising chitosan-coated alginate-tween 80 nanoparticles as rifampicin coadministered ascorbic acid delivery carrier against mycobacterium tuberculosis," 2019.

**11.** M. Damavandi, “Preparaiton of sodium alginate nanoparticles containing bovin serum albomin ( BSA ),” no. March, 2017.

**12.** P. Li, Y. Dai, J. Zhang, A. Wang, and Q. Wei, “Chitosan-alginate nanoparticles as a novel drug delivery system for nifedipine,” vol. 4, no. 3, pp. 221–228, 2008.

**13.** H. H. Volunteers, “Enhanced water dispersibility of curcumin encapsulated in alginate-polysorbate 80 nano particles and bioavailability in healthy human volunteers,” pp. 39–56, 2019.

**14.** H. Song et al., “Folic acid-chitosan conjugated nanoparticles for improving tumor-targeted drug delivery,” vol. 2013, 2013.

**15.** L. Brannon-Peppas and J. O. Blanchette, “Nanoparticle and targeted systems for cancer therapy,” Adv. Drug Deliv. Rev., vol. 64, no. SUPPL., pp. 206–212, 2012.

**16.** R. Singh, P. Thakur, A. Thakur, H. Kumar, and P. Chawla, “International Journal of Environmental Analytical Colorimetric sensing approaches of surface- modified gold and silver nanoparticles for detection of residual pesticides : a review,” Int. J. Environ. Anal. Chem., vol. 00, no. 00, pp. 1–17, 2020.

**17.** A. Manuscript, “Materials Chemistry B,” 2014.

**18.** M. T. Cook, G. Tzortzis, D. Charalampopoulos, and V. V Khutoryanskiy, “Production and evaluation of dry alginate-chitosan microcapsules as an enteric delivery vehicle for probiotic bacteria,” pp. 2834–2840, 2011.

**19.** G. Liu, M. Swierczewska, S. Lee, and X. Chen, “Functional nanoparticles for molecular imaging guided gene delivery,” Nano Today, vol. 5, no. 6, pp. 524–539, 2010.

**20.** M. Sook et al., “Tumor-homing glycol chitosan / polyethylenimine nanoparticles for the systemic delivery of siRNA in tumor-bearing mice,” J. Control. Release, vol. 144, no. 2, pp. 134–143, 2010.

**21.** J. Ji, D. Wu, L. Liu, J. Chen, and Y. Xu, “with methotrexate for targeted delivery,” pp. 1707–1720, 2012.

**22.** R. Sanivarapu, V. Vallabhaneni, and V. Verma, “The potential of curcumin in treatment of spinal cord injury,” Neurol. Res. Int., vol. 2016, pp. 1–11, 2016.

**23.** "The effects of Curcuma longa and curcumin on reproductive systems," vol. 51, no. 4, pp. 220–228, 2017.

**24.** Y. He, Y. Yue, X. Zheng, K. Zhang, S. Chen, and Z. Du, "Curcumin, inflammation, and chronic diseases: How are," pp. 9183–9213, 2015.

**25.** M. Naganuma, A. Saruwatari, S. Okamura, and H. Tamura, "Turmeric and curcumin modulate the conjugation of 1-Naphthol in caco-2 cells," Biol. Pharm. Bull., vol. 29, no. 7, pp. 1476–1479, 2006.

**26.** S. Bisht et al., "a novel strategy for human cancer therapy," vol. 18, pp. 1–18, 2007.

**27.** N. Inchai, Y. Ezure, D. Hongwiset, and S. Yotsawimonwat, "Investigation on solubility And stability of curcumin," vol. 60, pp. 91–95, 2015.

**28.** D. D. M. Carvalho, K. P. Takeuchi, R. M. Geraldine, C. J. De Moura, M. Célia, and L. Torres, "Production , solubility and antioxidant activity of curcumin nanosuspension," vol. 35, no. 1, pp. 115–119, 2015.

**29.** S. M. I. Morsy, "Review Article Role of Surfactants in Nanotechnology and Their Applications," vol. 3, no. 5, pp. 237–260, 2014.

**30.** E. M. Ahmed, "Hydrogel: Preparation, characterization, and applications: A review," J. Adv. Res., vol. 6, no. 2, pp. 105–121, 2015.

**31.** Chatterjee, S., Hui, P., & Kan, C. (2018). Thermoresponsive hydrogels and their biomedical applications: Special insight into their applications in textile based transdermal therapy. Polymers, 10(5), 480. doi:10.3390/polym10050480

**32.** Liu, M., Zeng, X., Ma, C., Yi, H., Ali, Z., Mou, X., . . . He, N. (2017). Injectable hydrogels for cartilage and bone tissue engineering. Bone Research, 5(1). doi:10.1038/boneres.2017.14

**33.** D. Han, Z. Lu, S. A. Chester, and H. Lee, "Micro 3D printing of a temperature-responsive hydrogel using projection micro-stereolithography," Sci. Rep., no. January, pp. 1–10, 2018.

**34.** J. Zhang, S. Huang, Y. Xue, and R. Zhuo, "Poly ( N -isopropylacrylamide ) nanoparticle- incorporated PNIPAAm hydrogels with fast shrinking kinetics," pp. 1346–1350, 2005.

**35.** J. Verma, J. Kanoujia, P. Parashar, C. B. Tripathi, and S. A. Saraf, "Wound healing applications of sericin/chitosan-capped silver nanoparticles incorporated hydrogel," Drug Deliv. Transl. Res., vol. 7, no. 1, pp. 77–88, 2017.

**36.** S. K. Leslie, R. C. Kinney, Z. Schwartz, and B. D. Boyan, "Chapter 20 Microencapsulation of stem cells for therapy," vol. 1479, pp. 251–259, 2017.

**37.** "Enhanced water dispersibility of curcumin encapsulated in alginate-polysorbate 80 for curcumin.pdf." .

**38.** D. Press, "Anti- Toxoplasma activity of various molecular weights and concentrations of chitosan nanoparticles on tachyzoites of RH strain," pp. 1341–1351, 2018.

**39.** Kiss, M. Z., Hobson, M. A., Varghese, T., Harter, J., Kliewer, M. A., Hartenbach, E. M., & Zagzebski, J. A. (2006). Frequency-dependent complex modulus of the uterus: Preliminary results. Physics in Medicine and Biology, 51(15), 3683-3695. doi:10.1088/0031-9155/51/15/006

# 8. APPENDICES

Appendix 1: Degradation evaluation of thermo-responsive pNIPAM hydrogel scaffolds

| Point Index | Sample Description | Action Name | Time (sequence) (s) | Time (action)( s) | Temp (Â°C) | Frequency (Hz) | Complex shear strain (%) | Complex shear stress (Pa) | Shear modulus (complex component) (Pa) | Shear modulus (elastic component) (Pa) | Shear modulus (viscous component) (Pa) | Shear viscosity (complex component) (Pa s) | Phase angle (Â°) | Normal force (N) | First normal stress difference (Pa) | Gap (mm) | Torque (Nm) | Absolute position (rad) | Harmonic distortion (%) |
|---|---|---|---|---|---|---|---|---|---|---|---|---|---|---|---|---|---|---|---|
| 1 | Control | Oscillation Amplitude | 343,1 | 25 | 40,03 | 1 | 1,07E-03 | 0,1002 | 9,33E+03 | 6,93E+03 | 6,25E+03 | 1,49E+03 | 42,04 | 0,2258 | | 0,85 | 2,10E-07 | 5,938 | 10,03 |
| 2 | Control | Oscillation Amplitude | 368,2 | 50,02 | 40,03 | 1 | 1,31E-03 | 0,1262 | 9,62E+03 | 7,01E+03 | 6,58E+03 | 1,53E+03 | 43,21 | 0,2188 | | 0,85 | 2,64E-07 | 5,938 | 5,933 |
| 3 | Control | Oscillation Amplitude | 393,2 | 75,04 | 40,02 | 1 | 1,57E-03 | 0,1588 | 1,01E+04 | 7,06E+03 | 7,22E+03 | 1,61E+03 | 45,63 | 0,2137 | | 0,85 | 3,33E-07 | 5,938 | 2,159 |
| 4 | Control | Oscillation Amplitude | 418,2 | 100,1 | 40,02 | 1 | 1,99E-03 | 0,1999 | 1,01E+04 | 7,09E+03 | 7,13E+03 | 1,60E+03 | 45,15 | 0,2079 | | 0,85 | 4,19E-07 | 5,938 | 1,6 |
| 5 | Control | Oscillation Amplitude | 443,2 | 125,1 | 40,01 | 1 | 2,48E-03 | 0,2517 | 1,02E+04 | 7,14E+03 | 7,22E+03 | 1,62E+03 | 45,34 | 0,1996 | | 0,85 | 5,27E-07 | 5,938 | 1,159 |
| 6 | Control | Oscillation Amplitude | 468,2 | 150,1 | 40,01 | 1 | 3,12E-03 | 0,3168 | 1,02E+04 | 7,15E+03 | 7,20E+03 | 1,62E+03 | 45,2 | 0,1992 | | 0,85 | 6,64E-07 | 5,938 | 1,991 |
| 7 | Control | Oscillation Amplitude | 493,2 | 175,1 | 40,01 | 1 | 3,88E-03 | 0,3989 | 1,03E+04 | 7,23E+03 | 7,31E+03 | 1,64E+03 | 45,35 | 0,1935 | | 0,85 | 8,35E-07 | 5,938 | 0,9093 |
| 8 | Control | Oscillation Amplitude | 518,3 | 200,1 | 40,01 | 1 | 4,83E-03 | 0,5021 | 1,04E+04 | 7,30E+03 | 7,41E+03 | 1,66E+03 | 45,42 | 0,1887 | | 0,85 | 1,05E-06 | 5,938 | 0,5081 |
| 9 | Control | Oscillation Amplitude | 543,3 | 225,1 | 40,01 | 1 | 6,03E-03 | 0,6321 | 1,05E+04 | 7,37E+03 | 7,45E+03 | 1,67E+03 | 45,31 | 0,1833 | | 0,85 | 1,32E-06 | 5,938 | 0,3179 |
| 10 | Control | Oscillation Amplitude | 568,3 | 250,1 | 40,01 | 1 | 7,59E-03 | 0,7958 | 1,05E+04 | 7,37E+03 | 7,45E+03 | 1,67E+03 | 45,33 | 0,1778 | | 0,85 | 1,67E-06 | 5,937 | 0,3859 |
| 11 | Control | Oscillation Amplitude | 593,3 | 275,2 | 40,01 | 1 | 9,60E-03 | 1,002 | 1,04E+04 | 7,31E+03 | 7,44E+03 | 1,66E+03 | 45,5 | 0,177 | | 0,85 | 2,10E-06 | 5,937 | 1,29 |
| 12 | Control | Oscillation Amplitude | 618,3 | 300,2 | 40,01 | 1 | 0,011829 | 1,261 | 1,07E+04 | 7,52E+03 | 7,56E+03 | 1,70E+03 | 45,15 | 0,1705 | | 0,85 | 2,64E-06 | 5,937 | 0,518 |
| 13 | Control | Oscillation Amplitude | 643,3 | 325,2 | 40,01 | 1 | 0,014896 | 1,588 | 1,07E+04 | 7,51E+03 | 7,56E+03 | 1,70E+03 | 45,21 | 0,1669 | | 0,85 | 3,33E-06 | 5,937 | 0,193 |
| 14 | Control | Oscillation Amplitude | 668,4 | 350,2 | 40,01 | 1 | 0,018683 | 1,999 | 1,07E+04 | 7,54E+03 | 7,59E+03 | 1,70E+03 | 45,21 | 0,1641 | | 0,85 | 4,19E-06 | 5,937 | 0,2585 |
| 15 | Control | Oscillation Amplitude | 693,4 | 375,2 | 40,01 | 1 | 0,023449 | 2,516 | 1,07E+04 | 7,56E+03 | 7,62E+03 | 1,71E+03 | 45,23 | 0,1613 | | 0,85 | 5,27E-06 | 5,937 | 0,1782 |
| 16 | Control | Oscillation Amplitude | 718,4 | 400,2 | 40,01 | 1 | 0,029385 | 3,168 | 1,08E+04 | 7,60E+03 | 7,64E+03 | 1,72E+03 | 45,14 | 0,1565 | | 0,85 | 6,64E-06 | 5,937 | 0,2004 |
| 17 | Control | Oscillation Amplitude | 743,4 | 425,3 | 40,02 | 1 | 0,036866 | 3,988 | 1,08E+04 | 7,63E+03 | 7,67E+03 | 1,72E+03 | 45,13 | 0,1532 | | 0,85 | 8,35E-06 | 5,937 | 0,2101 |
| 18 | Control | Oscillation Amplitude | 768,4 | 450,3 | 40,02 | 1 | 0,046332 | 5,021 | 1,08E+04 | 7,63E+03 | 7,70E+03 | 1,73E+03 | 45,28 | 0,149 | | 0,85 | 1,05E-05 | 5,937 | 0,1036 |
| 19 | Control | Oscillation Amplitude | 793,4 | 475,3 | 40,02 | 1 | 0,058191 | 6,321 | 1,09E+04 | 7,65E+03 | 7,71E+03 | 1,73E+03 | 45,21 | 0,1466 | | 0,85 | 1,32E-05 | 5,937 | 0,1065 |
| 20 | Control | Oscillation Amplitude | 818,5 | 500,3 | 40,01 | 1 | 0,073125 | 7,957 | 1,09E+04 | 7,67E+03 | 7,72E+03 | 1,73E+03 | 45,21 | 0,1432 | | 0,85 | 1,67E-05 | 5,938 | 0,1372 |
| 21 | Control | Oscillation Amplitude | 843,5 | 525,3 | 40,01 | 1 | 0,092046 | 10,02 | 1,09E+04 | 7,65E+03 | 7,74E+03 | 1,73E+03 | 45,31 | 0,14 | | 0,85 | 2,10E-05 | 5,938 | 0,1505 |
| 22 | Control | Oscillation Amplitude | 868,5 | 550,4 | 40,01 | 1 | 0,115886 | 12,61 | 1,09E+04 | 7,66E+03 | 7,73E+03 | 1,73E+03 | 45,29 | 0,139 | | 0,85 | 2,64E-05 | 5,938 | 0,2113 |
| 23 | Control | Oscillation Amplitude | 893,5 | 575,4 | 40,01 | 1 | 0,146219 | 15,88 | 1,09E+04 | 7,63E+03 | 7,73E+03 | 1,73E+03 | 45,37 | 0,1347 | | 0,85 | 3,33E-05 | 5,938 | 0,2689 |
| 24 | Control | Oscillation Amplitude | 918,5 | 600,4 | 40 | 1 | 0,18475 | 19,99 | 1,08E+04 | 7,59E+03 | 7,71E+03 | 1,72E+03 | 45,43 | 0,1316 | | 0,85 | 4,19E-05 | 5,938 | 0,3447 |
| 25 | Control | Oscillation Amplitude | 943,5 | 625,4 | 40,01 | 1 | 0,2338 | 25,16 | 1,08E+04 | 7,53E+03 | 7,69E+03 | 1,71E+03 | 45,59 | 0,1297 | | 0,85 | 5,27E-05 | 5,938 | 0,3862 |
| 26 | Control | Oscillation Amplitude | 968,6 | 650,4 | 40 | 1 | 0,296723 | 31,68 | 1,07E+04 | 7,45E+03 | 7,65E+03 | 1,70E+03 | 45,77 | 0,1257 | | 0,85 | 6,64E-05 | 5,938 | 0,4088 |
| 27 | Control | Oscillation Amplitude | 993,6 | 675,4 | 40,01 | 1 | 0,377911 | 39,88 | 1,06E+04 | 7,33E+03 | 7,59E+03 | 1,68E+03 | 45,99 | 0,1256 | | 0,85 | 8,35E-05 | 5,938 | 0,436 |
| 28 | Control | Oscillation Amplitude | 1,02E+03 | 700,5 | 40 | 1 | 0,483017 | 50,21 | 1,04E+04 | 7,18E+03 | 7,52E+03 | 1,65E+03 | 46,35 | 0,1195 | | 0,85 | 1,05E-04 | 5,938 | 0,405 |
| 29 | Control | Oscillation Amplitude | 1,04E+03 | 725,5 | 40,01 | 1 | 0,621764 | 63,21 | 1,02E+04 | 6,95E+03 | 7,42E+03 | 1,62E+03 | 46,89 | 0,1202 | | 0,85 | 1,32E-04 | 5,938 | 0,4799 |
| 30 | Control | Oscillation Amplitude | 1,07E+03 | 750,5 | 40 | 1 | 0,807525 | 79,58 | 9,86E+03 | 6,65E+03 | 7,28E+03 | 1,57E+03 | 47,6 | 0,1162 | | 0,85 | 1,67E-04 | 5,938 | 0,7613 |
| 31 | Control | Oscillation Amplitude | 1,09E+03 | 775,5 | 40 | 1 | 0,817796 | 80,15 | 9,80E+03 | 6,59E+03 | 7,26E+03 | 1,56E+03 | 47,78 | 0,1168 | | 0,85 | 1,68E-04 | 5,938 | 0,7597 |

**Figure 41.** Degredation evaluation of control pNIPAM hydrogel scaffolds with rheometer

| Point Index | Sample Description | Action Name | Time (sequence)(s) | Time (action) (s) | Temp (Â°C) | Frequency (Hz) | Complex shear strain (%) | Complex shear stress (Pa) | Shear modulus (complex component) (Pa) | Shear modulus (elastic component) (Pa) | Shear modulus (viscous component) (Pa) | Shear viscosity (complex component) (Pa s) | Phase angle (Â°) | Normal force (N) | First normal stress difference (Pa) | Gap (mm) | Torque (Nm) | Absolute position (rad) | Harmonic distortion (%) |
|---|---|---|---|---|---|---|---|---|---|---|---|---|---|---|---|---|---|---|---|
| 1 | P1 | Oscillation Amplitude | 25,2 | 25 | 40,02 | 1 | 2,27E-03 | 0,1002 | 4,42E+03 | 3,39E+03 | 2,84E+03 | 703,7 | 39,95 | -4,38E-03 | | 0,3 | 2,10E-07 | 5,93 | 7,543 |
| 2 | P1 | Oscillation Amplitude | 50,22 | 50,02 | 40,03 | 1 | 2,75E-03 | 0,1261 | 4,59E+03 | 3,57E+03 | 2,89E+03 | 731 | 39,02 | -7,30E-03 | | 0,3 | 2,64E-07 | 5,93 | 26,08 |
| 3 | P1 | Oscillation Amplitude | 75,24 | 75,04 | 40,02 | 1 | 3,41E-03 | 0,1587 | 4,65E+03 | 3,59E+03 | 2,95E+03 | 740,2 | 39,46 | -6,74E-03 | | 0,3 | 3,33E-07 | 5,93 | 6,628 |
| 4 | P1 | Oscillation Amplitude | 100,3 | 100,1 | 40,01 | 1 | 3,97E-03 | 0,1998 | 5,03E+03 | 3,85E+03 | 3,24E+03 | 800,6 | 40,11 | -0,0103 | | 0,3 | 4,19E-07 | 5,93 | 10,27 |
| 5 | P1 | Oscillation Amplitude | 125,3 | 125,1 | 40 | 1 | 5,51E-03 | 0,2516 | 4,57E+03 | 3,62E+03 | 2,79E+03 | 726,8 | 37,64 | -9,80E-03 | | 0,3 | 5,27E-07 | 5,93 | 22,8 |
| 6 | P1 | Oscillation Amplitude | 150,3 | 150,1 | 40 | 1 | 6,17E-03 | 0,3167 | 5,13E+03 | 3,95E+03 | 3,28E+03 | 817,1 | 39,68 | -0,0125 | | 0,3 | 6,63E-07 | 5,93 | 4,314 |
| 7 | P1 | Oscillation Amplitude | 175,3 | 175,1 | 40,01 | 1 | 7,85E-03 | 0,3987 | 5,08E+03 | 3,92E+03 | 3,23E+03 | 808 | 39,51 | -0,01545 | | 0,3 | 8,35E-07 | 5,93 | 2,388 |
| 8 | P1 | Oscillation Amplitude | 200,3 | 200,1 | 40,02 | 1 | 9,92E-03 | 0,5019 | 5,06E+03 | 3,91E+03 | 3,20E+03 | 805 | 39,3 | -0,01481 | | 0,3 | 1,05E-06 | 5,93 | 2,051 |
| 9 | P1 | Oscillation Amplitude | 225,3 | 225,1 | 40 | 1 | 0,012249 | 0,6319 | 5,16E+03 | 4,00E+03 | 3,26E+03 | 821 | 39,24 | -0,01687 | | 0,3 | 1,32E-06 | 5,93 | 0,9446 |
| 10 | P1 | Oscillation Amplitude | 250,4 | 250,2 | 39,99 | 1 | 0,015459 | 0,7955 | 5,15E+03 | 3,99E+03 | 3,26E+03 | 819 | 39,25 | -0,01791 | | 0,3 | 1,67E-06 | 5,93 | 1,257 |
| 11 | P1 | Oscillation Amplitude | 275,4 | 275,2 | 40 | 1 | 0,019091 | 1,001 | 5,25E+03 | 4,09E+03 | 3,28E+03 | 834,9 | 38,76 | -0,02014 | | 0,3 | 2,10E-06 | 5,93 | 0,7703 |
| 12 | P1 | Oscillation Amplitude | 300,4 | 300,2 | 40 | 1 | 0,023996 | 1,261 | 5,25E+03 | 4,10E+03 | 3,28E+03 | 836,2 | 38,66 | -0,01972 | | 0,3 | 2,64E-06 | 5,93 | 1,027 |
| 13 | P1 | Oscillation Amplitude | 325,4 | 325,2 | 40 | 1 | 0,030282 | 1,587 | 5,24E+03 | 4,08E+03 | 3,30E+03 | 834,2 | 38,95 | -0,02409 | | 0,3 | 3,32E-06 | 5,93 | 0,3678 |
| 14 | P1 | Oscillation Amplitude | 350,4 | 350,2 | 40 | 1 | 0,038548 | 1,998 | 5,18E+03 | 4,03E+03 | 3,26E+03 | 825 | 38,91 | -0,02543 | | 0,3 | 4,19E-06 | 5,93 | 0,2173 |
| 15 | P1 | Oscillation Amplitude | 375,5 | 375,2 | 40 | 1 | 0,048673 | 2,516 | 5,17E+03 | 4,01E+03 | 3,26E+03 | 822,5 | 39,06 | -0,02711 | | 0,3 | 5,27E-06 | 5,93 | 0,3877 |
| 16 | P1 | Oscillation Amplitude | 400,5 | 400,3 | 40,01 | 1 | 0,061573 | 3,167 | 5,14E+03 | 3,98E+03 | 3,25E+03 | 818,6 | 39,24 | -0,0284 | | 0,3 | 6,63E-06 | 5,93 | 0,3688 |
| 17 | P1 | Oscillation Amplitude | 425,5 | 425,3 | 40,01 | 1 | 0,078339 | 3,987 | 5,09E+03 | 3,94E+03 | 3,22E+03 | 810 | 39,26 | -0,03104 | | 0,3 | 8,35E-06 | 5,93 | 0,4369 |
| 18 | P1 | Oscillation Amplitude | 450,5 | 450,3 | 39,99 | 1 | 0,100703 | 5,019 | 4,98E+03 | 3,84E+03 | 3,18E+03 | 793,3 | 39,69 | -0,03425 | | 0,3 | 1,05E-05 | 5,93 | 0,4498 |
| 19 | P1 | Oscillation Amplitude | 475,5 | 475,3 | 40 | 1 | 0,129678 | 6,319 | 4,87E+03 | 3,72E+03 | 3,14E+03 | 775,6 | 40,17 | -0,0356 | | 0,3 | 1,32E-05 | 5,93 | 0,4484 |
| 20 | P1 | Oscillation Amplitude | 500,5 | 500,3 | 39,99 | 1 | 0,163019 | 7,955 | 4,88E+03 | 3,68E+03 | 3,21E+03 | 776,7 | 41,13 | -0,03575 | | 0,3 | 1,67E-05 | 5,93 | 0,6942 |
| 21 | P1 | Oscillation Amplitude | 525,6 | 525,4 | 40,01 | 1 | 0,213889 | 10,02 | 4,68E+03 | 3,49E+03 | 3,12E+03 | 745,2 | 41,82 | -0,03539 | | 0,3 | 2,10E-05 | 5,93 | 0,8347 |
| 22 | P1 | Oscillation Amplitude | 550,6 | 550,4 | 40 | 1 | 0,312391 | 12,61 | 4,04E+03 | 2,93E+03 | 2,78E+03 | 642,5 | 43,45 | -0,03716 | | 0,3 | 2,64E-05 | 5,93 | 0,9343 |
| 23 | P1 | Oscillation Amplitude | 575,6 | 575,4 | 40 | 1 | 0,471427 | 15,88 | 3,37E+03 | 2,33E+03 | 2,43E+03 | 536,1 | 46,23 | -0,03996 | | 0,3 | 3,33E-05 | 5,93 | 1,478 |
| 24 | P1 | Oscillation Amplitude | 600,6 | 600,4 | 40 | 1 | 1,00944 | 20,01 | 1,98E+03 | 1,11E+03 | 1,64E+03 | 315,4 | 56,05 | -0,03921 | | 0,3 | 4,19E-05 | 5,931 | 3,516 |
| 25 | P1 | Oscillation Amplitude | 625,6 | 625,4 | 40 | 1 | 98,4552 | 21,75 | 22,09 | 3,578 | 21,8 | 3,516 | 90 | -0,03945 | | 0,3 | 4,56E-05 | 5,833 | 6,653 |
| 26 | P1 | Oscillation Amplitude | 650,6 | 650,4 | 40,01 | 1 | 233,163 | 20,52 | 8,803 | 0,6672 | 8,777 | 1,401 | 90 | -0,04068 | | 0,3 | 4,30E-05 | 5,687 | 3,334 |
| 27 | P1 | Oscillation Amplitude | 675,7 | 675,4 | 40 | 1 | 358,948 | 17,61 | 4,906 | 0,2787 | 4,898 | 0,7808 | 90 | -0,04202 | | 0,3 | 3,69E-05 | 5,541 | 1,883 |
| 28 | P1 | Oscillation Amplitude | 700,7 | 700,5 | 40 | 1 | 483,631 | 15,52 | 3,209 | 0,1833 | 3,204 | 0,5108 | 90 | -0,04172 | | 0,3 | 3,25E-05 | 5,441 | 1,27 |
| 29 | P1 | Oscillation Amplitude | 725,7 | 725,5 | 40 | 1 | 626,864 | 14,06 | 2,242 | 0,1414 | 2,238 | 0,3569 | 90 | -0,04264 | | 0,3 | 2,94E-05 | 5,347 | 0,8578 |

**Figure 42.** Degredation evaluation of P1 incorporated pNIPAM hydrogel scaffolds with rheometer

| Point Index | Sample Description | Action Name | Time (sequence)(s) | Time (action)(s) | Temp (Â°C) | Frequency (Hz) | Complex shear strain(%) | Complex shear stress(Pa) | Shear modulus (complex component)(Pa) | Shear modulus (elastic component)(Pa) | Shear modulus (viscous component)(Pa) | Shear viscosity (complex component)(Pa s) | Phase angle(Â°) | Normal force(N) | First normal stress difference(Pa) | Gap(mm) | Torque (N m) | Absolute position(rad) | Harmonic distortion(%) |
|---|---|---|---|---|---|---|---|---|---|---|---|---|---|---|---|---|---|---|---|
| 1 | P5 | Oscillation Amplitude | 25,28 | 25 | 40,1 | 1 | 1,49E-03 | 0,1002 | 6,70E+03 | 5,07E+03 | 4,38E+03 | 1,07E+03 | 40,86 | 0,01494 | | 0,5 | 2,10E-07 | 5,941 | 10,86 |
| 2 | P5 | Oscillation Amplitude | 50,34 | 50,06 | 40,09 | 1 | 2,10E-03 | 0,1262 | 6,00E+03 | 4,77E+03 | 3,63E+03 | 954,6 | 37,29 | 0,01307 | | 0,5 | 2,64E-07 | 5,941 | 16,48 |
| 3 | P5 | Oscillation Amplitude | 75,35 | 75,07 | 40,08 | 1 | 2,41E-03 | 0,1588 | 6,59E+03 | 5,17E+03 | 4,09E+03 | 1,05E+03 | 38,33 | 0,01312 | | 0,5 | 3,33E-07 | 5,941 | 6,971 |
| 4 | P5 | Oscillation Amplitude | 100,4 | 100,1 | 40,08 | 1 | 3,13E-03 | 0,1999 | 6,39E+03 | 5,09E+03 | 3,87E+03 | 1,02E+03 | 37,24 | 0,01191 | | 0,5 | 4,19E-07 | 5,941 | 2,855 |
| 5 | P5 | Oscillation Amplitude | 125,4 | 125,1 | 40,06 | 1 | 3,93E-03 | 0,2517 | 6,41E+03 | 5,11E+03 | 3,87E+03 | 1,02E+03 | 37,11 | 8,41E-03 | | 0,5 | 5,27E-07 | 5,941 | 1,687 |
| 6 | P5 | Oscillation Amplitude | 150,4 | 150,1 | 40,05 | 1 | 4,84E-03 | 0,3168 | 6,55E+03 | 5,22E+03 | 3,96E+03 | 1,04E+03 | 37,17 | 8,21E-03 | | 0,5 | 6,64E-07 | 5,941 | 2,93 |
| 7 | P5 | Oscillation Amplitude | 175,4 | 175,1 | 40,04 | 1 | 5,80E-03 | 0,3989 | 6,88E+03 | 5,52E+03 | 4,11E+03 | 1,10E+03 | 36,71 | 6,46E-03 | | 0,5 | 8,35E-07 | 5,941 | 4,751 |
| 8 | P5 | Oscillation Amplitude | 200,4 | 200,2 | 40,03 | 1 | 7,24E-03 | 0,5021 | 6,94E+03 | 5,54E+03 | 4,18E+03 | 1,10E+03 | 37 | 3,37E-03 | | 0,5 | 1,05E-06 | 5,941 | 1,444 |
| 9 | P5 | Oscillation Amplitude | 225,5 | 225,2 | 40,04 | 1 | 9,15E-03 | 0,6321 | 6,91E+03 | 5,50E+03 | 4,17E+03 | 1,10E+03 | 37,15 | 1,72E-03 | | 0,5 | 1,32E-06 | 5,941 | 0,7755 |
| 10 | P5 | Oscillation Amplitude | 250,5 | 250,2 | 40,04 | 1 | 0,0121055 | 0,7959 | 6,58E+03 | 5,22E+03 | 4,00E+03 | 1,05E+03 | 37,45 | 1,54E-03 | | 0,5 | 1,67E-06 | 5,941 | 0,8197 |
| 11 | P5 | Oscillation Amplitude | 275,5 | 275,2 | 40,05 | 1 | 0,0152076 | 1,002 | 6,59E+03 | 5,24E+03 | 3,99E+03 | 1,05E+03 | 37,32 | 2,94E-05 | | 0,5 | 2,10E-06 | 5,941 | 0,4726 |
| 12 | P5 | Oscillation Amplitude | 300,5 | 300,2 | 40,03 | 1 | 0,0196229 | 1,261 | 6,43E+03 | 5,11E+03 | 3,91E+03 | 1,02E+03 | 37,4 | -3,57E-03 | | 0,5 | 2,64E-06 | 5,941 | 1,702 |
| 13 | P5 | Oscillation Amplitude | 325,5 | 325,2 | 40,03 | 1 | 0,0245332 | 1,588 | 6,47E+03 | 5,13E+03 | 3,95E+03 | 1,03E+03 | 37,62 | -4,17E-03 | | 0,5 | 3,33E-06 | 5,941 | 0,7636 |
| 14 | P5 | Oscillation Amplitude | 350,5 | 350,3 | 40,02 | 1 | 0,030821 | 1,999 | 6,49E+03 | 5,16E+03 | 3,93E+03 | 1,03E+03 | 37,31 | -5,30E-03 | | 0,5 | 4,19E-06 | 5,941 | 0,3635 |
| 15 | P5 | Oscillation Amplitude | 375,6 | 375,3 | 40,01 | 1 | 0,0393056 | 2,517 | 6,40E+03 | 5,05E+03 | 3,93E+03 | 1,02E+03 | 37,88 | -6,71E-03 | | 0,5 | 5,27E-06 | 5,941 | 0,721 |
| 16 | P5 | Oscillation Amplitude | 400,6 | 400,3 | 40,02 | 1 | 0,0495871 | 3,169 | 6,39E+03 | 5,08E+03 | 3,88E+03 | 1,02E+03 | 37,37 | -8,58E-03 | | 0,5 | 6,64E-06 | 5,941 | 0,6969 |
| 17 | P5 | Oscillation Amplitude | 425,6 | 425,3 | 40,01 | 1 | 0,0633089 | 3,989 | 6,30E+03 | 4,98E+03 | 3,86E+03 | 1,00E+03 | 37,77 | -0,01122 | | 0,5 | 8,36E-06 | 5,941 | 0,3792 |
| 18 | P5 | Oscillation Amplitude | 450,6 | 450,3 | 40,01 | 1 | 0,080931 | 5,022 | 6,21E+03 | 4,88E+03 | 3,84E+03 | 987,6 | 38,18 | -0,01243 | | 0,5 | 1,05E-05 | 5,941 | 0,392 |
| 19 | P5 | Oscillation Amplitude | 475,6 | 475,4 | 40,01 | 1 | 0,104829 | 6,323 | 6,03E+03 | 4,70E+03 | 3,78E+03 | 959,9 | 38,82 | -0,01298 | | 0,5 | 1,32E-05 | 5,941 | 0,5226 |
| 20 | P5 | Oscillation Amplitude | 500,6 | 500,4 | 40,01 | 1 | 0,134474 | 7,96 | 5,92E+03 | 4,58E+03 | 3,75E+03 | 942,1 | 39,34 | -0,01532 | | 0,5 | 1,67E-05 | 5,941 | 0,4863 |
| 21 | P5 | Oscillation Amplitude | 525,7 | 525,4 | 40,01 | 1 | 0,173817 | 10,02 | 5,77E+03 | 4,43E+03 | 3,69E+03 | 917,6 | 39,83 | -0,01639 | | 0,5 | 2,10E-05 | 5,941 | 0,5283 |
| 22 | P5 | Oscillation Amplitude | 550,7 | 550,4 | 40,01 | 1 | 0,205961 | 12,61 | 6,13E+03 | 4,68E+03 | 3,96E+03 | 974,8 | 40,23 | -0,01835 | | 0,5 | 2,64E-05 | 5,941 | 0,8638 |
| 23 | P5 | Oscillation Amplitude | 575,7 | 575,4 | 40,01 | 1 | 0,267476 | 15,88 | 5,94E+03 | 4,49E+03 | 3,88E+03 | 945 | 40,81 | -0,01953 | | 0,5 | 3,33E-05 | 5,942 | 0,9679 |
| 24 | P5 | Oscillation Amplitude | 600,7 | 600,4 | 40,01 | 1 | 0,37715 | 20 | 5,30E+03 | 3,97E+03 | 3,52E+03 | 843,9 | 41,6 | -0,02199 | | 0,5 | 4,19E-05 | 5,942 | 0,7124 |
| 25 | P5 | Oscillation Amplitude | 625,7 | 625,4 | 40,02 | 1 | 0,503958 | 25,18 | 5,00E+03 | 3,68E+03 | 3,38E+03 | 795,2 | 42,57 | -0,02416 | | 0,5 | 5,27E-05 | 5,942 | 0,9435 |
| 26 | P5 | Oscillation Amplitude | 650,7 | 650,5 | 40,02 | 1 | 0,702777 | 31,7 | 4,51E+03 | 3,22E+03 | 3,16E+03 | 718 | 44,41 | -0,02436 | | 0,5 | 6,64E-05 | 5,942 | 1,219 |
| 27 | P5 | Oscillation Amplitude | 675,8 | 675,5 | 40,03 | 1 | 1,11268 | 39,93 | 3,59E+03 | 2,42E+03 | 2,65E+03 | 571,2 | 47,61 | -0,02447 | | 0,5 | 8,36E-05 | 5,942 | 2,206 |
| 28 | P5 | Oscillation Amplitude | 700,8 | 700,5 | 40,02 | 1 | 7,50352 | 50,68 | 675,5 | 321,4 | 594,1 | 107,5 | 61,58 | -0,01854 | | 0,5 | 1,06E-04 | 5,946 | 14,58 |
| 29 | P5 | Oscillation Amplitude | 725,8 | 725,5 | 40,02 | 1 | 295,414 | 42,33 | 14,33 | 0,2797 | 14,33 | 2,281 | 88,88 | -0,01857 | | 0,5 | 8,87E-05 | 0,5831 | 3,059 |
| 30 | P5 | Oscillation Amplitude | 750,9 | 750,6 | 40,02 | 1 | 469,243 | 33,65 | 7,172 | 0,7672 | 7,131 | 1,141 | 83,86 | -0,01727 | | 0,5 | 7,05E-05 | 0,7642 | 1,85 |
| 31 | P5 | Oscillation Amplitude | 775,9 | 775,6 | 40,01 | 1 | 619,178 | 31,17 | 5,035 | 0,7557 | 4,978 | 0,8013 | 81,37 | -0,02076 | | 0,5 | 6,53E-05 | 0,7929 | 1,283 |



**Figure 43.** Degradation evaluation of P2 incorporated pNIPAM hydrogel scaffolds with rheometer

Appendix 2: Swelling capacity profiles of control hydrogel scaffold, P1 nanoparticles incorporated pNIPAM hydrogel scaffold, P2 nanoparticles incorporated pNIPAM hydrogel scaffold

**Table 3.** Swelling capacity profiles of control hydrogel scaffold

| C-3 (mg) | C-2 mg) | C-1 mg) | Time interval | Time (sec) |
|---|---|---|---|---|
| 24,7 | 25,5 | 30,6 | t0 | 0 |
| 74 | 52,7 | 48 | t1 | 30 |
| 60,9 | 42,3 | 43,6 | t2 | 60 |
| 53,6 | 37,7 | 44,4 | t3 | 90 |
| 46,2 | 37,4 | 45,4 | t4 | 150 |
| 45,1 | 37 | 43,2 | t5 | 210 |
| 45,9 | 37,1 | 42 | t6 | 270 |
| 43,7 | 35,3 | 43 | t7 | 390 |
| 44,1 | 35 | 39,5 | t8 | 510 |
| 45,6 | 34,7 | 38,3 | t9 | 630 |
| 44,6 | 34 | 37,3 | t10 | 930 |
| 45,5 | 33,7 | 36,3 | t11 | 1530 |
| 46,3 | 32,6 | 37,7 | t12 | 2430 |
| 45,7 | 33,9 | 37,2 | t13 | 4230 |
| 44,3 | 32,8 | 36,2 | t14 | 7830 |
| 43,7 | 32,9 | 36,4 | t15 | 11430 |
| 43,1 | 32 | 33,1 | t16 | 15030 |

| | | | | |
|---|---|---|---|---|
| 45,8 | 34,8 | 38,7 | t17 | 101430 |
| 41,9 | 33,9 | 29,6 | t19 | 187830 |
| 39,7 | 31,9 | 26,5 | t20 | 274230 |
| 39,7 | 32,4 | 25,6 | t21 | 11430 |
| 39,6 | 31,1 | 25,3 | t22 | 15030 |
| 38,3 | 30,5 | 24,7 | t23 | 101430 |
| 33,3 | 30,2 | 24,9 | t24 | 274230 |
| 30,3 | 30,5 | 24,3 | t25 | 360630 |

**Table 4.** Swelling capacity profiles of P1 nanoparticles incorporated pNIPAM hydrogel scaffold

| **P1-3 (mg)** | **P1-2 mg)** | **P1-1 mg)** | **Time interval** | **Time (sec)** |
|---|---|---|---|---|
| 22,4 | 27 | 29 | t0 | 0 |
| 42,7 | 51,6 | 77,9 | t1 | 30 |
| 36,8 | 44,8 | 62,4 | t2 | 60 |
| 32 | 44,7 | 57,8 | t3 | 90 |
| 30,4 | 44,2 | 52,4 | t4 | 150 |
| 28,4 | 44,3 | 48,8 | t5 | 210 |
| 28 | 42,9 | 46,9 | t6 | 270 |
| 24,8 | 42,5 | 47,1 | t7 | 390 |
| 25,5 | 42,1 | 44,4 | t8 | 510 |
| 23,4 | 42 | 46 | t9 | 630 |
| 22,7 | 40,6 | 46 | t10 | 930 |

| | | | | |
|---|---|---|---|---|
| 23 | 41,6 | 44,3 | t11 | 1530 |
| 20,9 | 40,1 | 41 | t12 | 2430 |
| 22,1 | 42,3 | 41,7 | t13 | 4230 |
| 21,5 | 37 | 38,3 | t14 | 7830 |
| 18,9 | 36 | 37,6 | t16 | 11430 |
| 20,3 | 41,7 | 41,5 | t17 | 15030 |
| 20,70 | 39,2 | 40,3 | t18 | 101430 |
| 18,7 | 33,5 | 33,6 | t19 | 187830 |
| 20,1 | 32,8 | 31,5 | t20 | 274230 |
| 17,7 | 30 | 28,2 | t21 | 11430 |
| 16,9 | 28,6 | 25 | t22 | 15030 |
| 16 | 27,9 | 25,3 | t23 | 101430 |
| 14,9 | 27,7 | 18,2 | t24 | 274230 |

**Table 5.** Swelling capacity profiles of P2 nanoparticles incorporated pNIPAM hydrogel scaffold

| **P2-3 (mg)** | **P2-2 (mg)** | **P2-1 (mg)** | **Time interval** | **Time (sec)** |
|---|---|---|---|---|
| 27,2 | 29,8 | 25,2 | t0 | 0 |
| 50,6 | 95,9 | 39,6 | t1 | 30 |
| 69,3 | 87 | 47,9 | t2 | 60 |
| 59,8 | 87,1 | 48,3 | t3 | 90 |
| 56 | 82,7 | 41 | t4 | 150 |
| 51,8 | 82,2 | 37,2 | t5 | 210 |
| 52,9 | 80,9 | 35,3 | t6 | 270 |
| 50,5 | 78,8 | 34,9 | t7 | 390 |
| 51,3 | 80,6 | 32,2 | t8 | 510 |
| 45,7 | 80,6 | 34,2 | t9 | 630 |
| 46,1 | 79,4 | 32,6 | t10 | 930 |
| 45,9 | 83,7 | 35,3 | t11 | 1530 |
| 45,5 | 79,2 | 31,2 | t12 | 2430 |
| 48,3 | 69,5 | 29,9 | t13 | 4230 |
| 44,5 | 56,9 | 30,6 | t14 | 7830 |
| 46,7 | 52,3 | 30,6 | t15 | 11430 |
| 40,7 | 47,5 | 28,4 | t16 | 15030 |
| 37,6 | 35,1 | 27,1 | t17 | 101430 |
| 36,1 | 38,2 | 26,6 | t18 | 187830 |
| 33,6 | 36,4 | 27,9 | t19 | 274230 |
| 31 | 30,4 | 26,4 | t20 | 11430 |

| | | | | |
|---|---|---|---|---|
| 28 | 26,9 | 24,9 | t21 | 15030 |
| 26,5 | 25,8 | 23,6 | t22 | 101430 |

# 9. CURRICULUM VITAE

**Personal Information**

| | | | |
|---|---|---|---|
| **Name** | Elif Gülin | **Surname** | Ertuğral |
| **Place of Birth** | | **Date of Birth** | |
| **Nationality** | | **Telephone Number** | |
| **E-mail** | | | |

**Education**

| | Institution Name | Graduation Year |
|---|---|---|
| **Master of Science** | Acibadem Mehmet Ali Aydinlar University, Institute of Science, M.Sc. in Medical Engineering | 2020 |
| **Undergraduate** | Marmara University, Faculty of Engineering, B.Sc. in Bioengineering Istanbul, Turkey | 2017 |
| **High School** | Aydın Süleyman Demirel Anatolian High School Aydın, Turkey | 2013 |

**Work Experience**

| Position | Corporation | Duration |
|---|---|---|
| Teaching Assistant | Acibadem Mehmet Ali Aydinlar University | Sep 2018 - Present |
| Process Development Intern | Turgut Pharmaceuticals | July - Sep 2018 |
| Import/Export Coordinator | Duayen Yapı Kimya San. Tic. A.S | Oct - May 2018 |
| Process Engineering Intern – Erasmus Traineeship | University of Szeged | July - Sep 2017 |
| Production Intern | KOEK Bioengineering Biotechnology and Medical Services Company | June – Aug 2016 |
| Microbiology Intern | Istanbul University Cerrahpasa | June-Aug 2015 |

**Foreign Languages**

| Language | Reading* | Speaking- | Writing* |
|---|---|---|---|
| English | Advanced | Advanced | Advanced |

| | | | |
|---|---|---|---|
| German | Intermediate | Intermediate | Intermediate |

***** Evaluated as advanced, good,intermediate,beginner

**Foreign Language Exam Results[#]**

| KPDS | ÜDS | IELTS | TOEFL IBT | TOEFL PBT | TOEFL CBT | DİĞER |
|---|---|---|---|---|---|---|
| | | | | | | **YÖKDİL** 83,75 |

KPDS: Kamu Personeli Yabancı Dil Sınavı; ÜDS: Üniversitelerarası Kurul Yabancı Dil Sınavı; IELTS: International English Language Testing System; TOEFL IBT: Test of English as a Foreign Language-Internet-Based Test TOEFL PBT: Test of English as a Foreign Language-Paper-Based Test; TOEFL CBT: Test of English as a Foreign Language-Computer- Based Test; FCE: First Certificate in English; CAE: Certificate in Advanced English; CPE: Certificate of Proficiency in English

**Other Exams**

| Name of the Exam | Quantitative | Equally Weighted | Verba |
|---|---|---|---|
| ALES** | 73 | | |

****** ALES: Akademik Personel ve Lisansüstü Eğitimi Giriş Sınavı

**Computer Skills**

| **Program** | **Ability to Use** |
|---|---|
| Microsoft Office | Advanced |
| Fusion 360 | Beginner |
| Matlab | Beginner |